

Hints, neutrino bounds, and WDM constraints from SDSS DR14 Lyman- α and Planck full-survey data

Nathalie Palanque-Delabrouille,^a Christophe Yèche,^a Nils Schöneberg,^b Julien Lesgourgues,^b Michael Walther,^a Solène Chabanier,^a Eric Armengaud^a

^a*IRFU, CEA, Université Paris-Saclay,*
F-91191 Gif-sur-Yvette, France

^b*RWTH Aachen University, Institute for Theoretical Particle Physics and Cosmology (TTK),*
Sommerfeldstrasse 16, 52074, Aachen, Germany

E-mail: nathalie.palanque-delabrouille@cea.fr, christophe.yeche@cea.fr,
schoeneberg@physik.rwth-aachen.de, lesgourg@physik.rwth-aachen.de,
michael.walther@cea.fr, solene.chabanier@cea.fr, eric.armengaud@cea.fr

Abstract. The Lyman- α forest 1D flux power spectrum is a powerful probe of several cosmological parameters. Assuming a Λ CDM cosmology including massive neutrinos, we find that the latest SDSS DR14 BOSS and eBOSS Lyman- α forest data is in very good agreement with current weak lensing constraints on (Ω_m, σ_8) and has the same small level of tension with Planck. We did not identify a systematic effect in the data analysis that could explain this small tension, but we show that it can be reduced in extended cosmological models where the spectral index is not the same on the very different times and scales probed by CMB and Lyman- α data. A particular case is that of a Λ CDM model including a running of the spectral index on top of massive neutrinos. With combined Lyman- α and Planck data, we find a slight (3σ) preference for negative running, $\alpha_s = -0.010 \pm 0.004$ (68%CL). Neutrino mass bounds are found to be robust against different assumptions. In the Λ CDM model with running, we find $\sum m_\nu < 0.11$ eV at the 95% confidence level for combined Lyman- α and Planck (temperature and polarisation) data, or $\sum m_\nu < 0.09$ eV when adding CMB lensing and BAO data. We further provide strong and nearly model-independent bounds on the mass of thermal warm dark matter. For a conservative configuration consisting of SDSS data restricted to $z < 4.5$ combined with XQ-100 Lyman- α data, we find $m_X > 5.3$ keV (95%CL).

Contents

1	Introduction	1
2	Data and Methodology	2
2.1	Data	3
2.1.1	Lyman- α forest 1D flux power spectrum	3
2.1.2	Cosmic microwave background	3
2.1.3	Baryon acoustic oscillations	3
2.2	Modeling of the Lyman- α forest 1D flux power spectrum	3
2.3	Interpretation methodology	7
2.3.1	Frequentist interpretation	7
2.3.2	Bayesian interpretation	8
3	Results	9
3.1	Cosmological constraints from Lyman- α data alone	10
3.2	Mild tension between Planck and Lyman- α data	11
3.3	Combining CMB and Lyman- α data	16
3.4	Λ CDM $\nu + \alpha_s$ cosmology	18
3.5	Neutrino mass bounds	20
3.6	Constraints on Λ WDM model	21
4	Conclusions	24
A	Thermal history	27
B	Correlation coefficients	29

1 Introduction

Modern cosmological experiments have delivered an impressive amount of high-quality data on several observables, related either to cosmic microwave background (CMB) anisotropies, to the Large Scale Structure of the Universe, or to its expansion history. In many cases, the measurements are so precise that the interpretation of the data is limited by systematic rather than statistical errors. Nevertheless, a consistent picture is emerging, with the minimal 6-parameter Λ CDM model standing out as the simplest explanation for most observations.

There are still very strong reasons for gathering more and better data. First, the current status of the Λ CDM model is not entirely clear, with intriguing and persistent hints of anomalies like the small-scale dark matter crisis, the Hubble tension, and the σ_8 tension. To better understand what is going on, we need to combine several types of observations, sensitive to different systematics. The comparison of different and independent probes is the best way to get a clue on the origin of these tensions. Second, on the basis of laboratory experiments and theoretical modelling, we believe that the total neutrino mass very likely impacts cosmological observables at a level which is not very far from the current detection threshold. Third, the possible detection of any signature beyond the simplest paradigm of

a cosmological constant, of some plain cold dark matter, of slow-roll inflation and Einstein’s gravity would have a very deep impact on our quest for new physics.

The Lyman- α forest flux power spectrum is a powerful tool to study clustering in the universe at redshifts 2 to 6, on scales that are strongly non-linear today, but were only mildly non-linear at such high redshifts. Since it extends the lever arm of other cosmological probes towards smaller scales, it has often been used to constraint the parameters of models affecting only the smallest scales – like warm dark matter (WDM) [1–4] or interacting dark matter [5–7] – or altering the global shape of the power spectrum – like non-slow-roll inflation or massive neutrino free-streaming [8, 9]. Recent data from the Lyman- α flux power spectrum provide some of the strongest existing bounds on the mass of WDM [10–14]. In combination with CMB data, they also provide the strongest cosmological neutrino mass bounds to date [15–19].

A new high precision measurement of the one-dimensional Lyman- α flux power spectrum was recently published [20], using 43 751 high-quality quasar spectra from the Data Release 14 of the BOSS and eBOSS collaborations [21, 22]. It covers thirteen redshift bins from $z = 2.2$ to 4.6, up to the wavenumber $k = 0.02 \text{ s km}^{-1}$. This work presents a first cosmological interpretation of this data set. For this purpose, we have assembled a grid of 138 hydrodynamical simulations with a resolution equivalent to 3×3072^3 particles in a $(100\text{Mpc}/h)^3$ box, which we obtain using a splicing technique, extending the grid from [23] used in previous work. We have built a likelihood for the new data set, and two analysis pipelines for cosmological parameter extraction.

In section 2.1 we describe the data sets that we employ in this work. In section 2.2 we explain our settings and assumptions for numerical simulations and for the astrophysical modeling of the intergalactic medium (IGM). In section 2.3 we have a short discussion on the frequentist and Bayesian interpretation methodologies. Our results are presented in section 3. We start from the analysis of Lyman- α data alone in section 3.1, and we discuss its compatibility with Planck and BAO data in section 3.2. In section 3.3 we combine the Lyman- α , CMB, and BAO data for the Λ CDM model with massive neutrinos, and we show that the compatibility between Lyman- α and Planck data could be improved in cosmological models where the effective slope of the spectrum is different on CMB and Lyman- α scales. In section 3.4 we present our bounds for an example of such a model, involving a running of the spectral index. We present our neutrino (resp. WDM) mass bounds and discuss their robustness in section 3.5 (resp. 3.6). Our conclusion are summarized in 4.

2 Data and Methodology

In this section, we first present the data sets we use. We then recall the modeling of the Lyman- α forest developed in earlier works and introduce several new improvements. We finally briefly describe the two interpretation methodologies used throughout this work, which allow us to test the robustness of the obtained results.

2.1 Data

2.1.1 Lyman- α forest 1D flux power spectrum

We use the 1D Lyman- α flux power spectrum measurement from PY15 [17], which is based on the DR14 BOSS and eBOSS data of the Sloan Digital Sky Survey (SDSS). The data consist of a subsample of 43 751 quasars selected from a parent sample of 180 413 quasars [24–27] according to the spectrum quality. This sample improves over the one from SDSS BOSS DR9 used in previous works both in statistical precision (achieving a reduction by a factor of two) and in redshift coverage. We now have 13 equally-spaced redshift bins covering the range from $z = 2.2$ to 4.6, as opposed to 12 bins from $z = 2.2$ to 4.4 in [28]. These data also come with systematic uncertainties that result from an in-depth study of relevant observational (resolution, noise, sky subtraction, continuum fitting) as well as astrophysical effects (damped Lyman- α systems, broad absorption lines, metal contamination). We thus perform the analysis on 435 Lyman- α data points, spread evenly over 35 bins in k space (from $k = 0.0011 \text{ s km}^{-1}$ to 0.0195 s km^{-1}) and 13 bins in redshift space. Figure 1 illustrates the SDSS DR14 Lyman- α 1D flux power spectrum measurement and the best-fit $\Lambda\text{CDM} + \sum m_\nu$ model of section 3.1.

We also explore an extended Lyman- α data set by considering the 1D Lyman- α flux power spectrum measurement from the one hundred XQ-100 quasars [19]. These data cover three redshift bins at $z = 3.2$, 3.6, and 3.9. They exhibit a better resolution than the SDSS data, and thus allow an extension of the analysis to slightly higher k modes, namely to $k = 0.05 \text{ s km}^{-1}$ for $z = 3.2$, $k = 0.06 \text{ s km}^{-1}$ for $z = 3.6$, and $k = 0.07 \text{ s km}^{-1}$ for $z = 3.9$.

2.1.2 Cosmic microwave background

For the CMB data, we use the Planck 2018 data sets. The likelihoods for the Bayesian approach are described in [29], and the corresponding publicly available chains are used for the frequentist approach. We always use the full low- ℓ and high- ℓ temperature and polarization data, denoted as “P18”. When specified, we also include the Planck 2018 CMB lensing data, denoted as “lens.”.

2.1.3 Baryon acoustic oscillations

We also combine CMB data with measurements of the BAO scale by 6dFGS [30], SDSS main galaxy sample [31], BOSS-LOWZ, and CMASS from DR12 [32]. These measurements are henceforth globally denoted “BAO”. The additional constraints that these measurement provide on cosmological parameters are included in the present work with their full correlation with CMB data. For the frequentist approach described in section 2.3.1, both CMB and BAO constraints are taken from the Markov chains publicly available through the official Planck legacy archive. For the Bayesian approach, the constraints are directly derived from the likelihoods available through MONTEPYTHON 3.

2.2 Modeling of the Lyman- α forest 1D flux power spectrum

To predict the theoretical Lyman- α flux power spectrum, we use the set of simulations extensively described in BP14 [23] for the initial grid, in [33] for the active neutrino sector and in

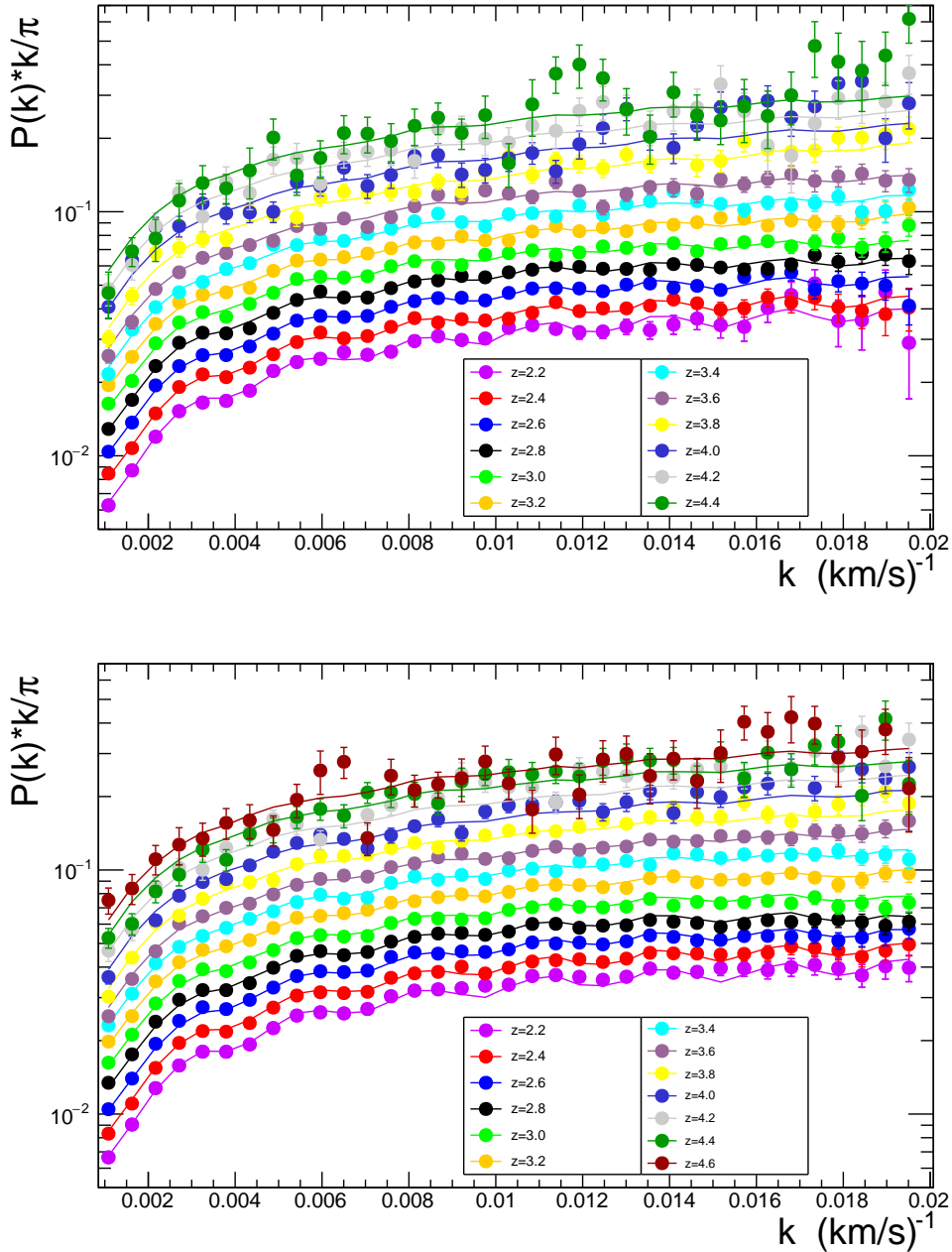


Figure 1. **Top:** BOSS DR9 Lyman- α data from [17] and best-fit Λ CDM + $\sum m_\nu$ model. **Bottom:** eBOSS DR14 Lyman- α data from [20] and best-fit Λ CDM + $\sum m_\nu$ model.

PY15 [17] for systematic studies related to these simulations. The WDM extension of the grid was introduced in [10]. We present here a brief summary. The simulations are run using a parallel tree smoothed particle hydrodynamics (tree-SPH) code GADGET-3, an updated version of the public code GADGET-2 [34, 35]. The simulations are started at $z = 30$, with initial transfer functions and power spectra computed with CAMB [36], and initial particle displace-

Parameter	Definition
Ω_m	Matter fraction today (compared to critical density)
H_0	Expansion rate today in $\text{km s}^{-1} \text{Mpc}^{-1}$
σ_8	RMS matter fluctuation amplitude today in linear theory
n_s	Scalar spectral index
$\sum m_\nu$	Sum of neutrino masses
m_X	Mass of thermal relic WDM particle
α_s	Running of the power spectrum scalar index
$T_0(z=3)$	Normalization temperature of IGM at $z=3$
$\gamma(z=3)$	Logarithmic slope of δ -dependence of IGM temperature at $z=3$
$\eta^T(z<3)$	Logarithmic slope of z -dependence of T_0 for $z<3$
$\eta^T(z>3)$	Logarithmic slope of z -dependence of T_0 for $z>3$
η^γ	Logarithmic slope of z -dependence of γ
A^τ	Amplitude of the effective optical depth of Ly α absorption τ_{eff}
η^τ	Logarithmic slope of redshift dependence of τ_{eff}
$f_{\text{Si III}}$	Fraction of Si III absorption relative to Ly α absorption
$f_{\text{Si II}}$	Fraction of Si II absorption relative to Ly α absorption
z_{reio}	Redshift of reionization
A^{splice}	Amplitude of splicing correction
η^{splice}	Small-scale slope of splicing correction
A^{SN}	Amplitude of supernova feedback correction
A^{AGN}	Amplitude of AGN feedback correction
A^{UVfluct}	Amplitude of UV fluctuation correction
$A^{n,i}$	Amplitude of noise power correction for redshift bin i

Table 1. Definition of the parameters used throughout this work, sorted in three categories: cosmological, astrophysical, and nuisance. The latter two sets of parameters describe corrections that are only applied to the Lyman- α flux power spectrum.

ments generated with second-order Lagrangian perturbation theory 2LPT¹. We include three particle types: collisionless dark matter, gas and, when relevant, mass-degenerate neutrinos. We showed in [28] that considering inverted or normal neutrino mass hierarchy yields a flux power spectrum that differs by less than 0.05% from the degenerate-mass scenario, a level ten times below the simulation statistical uncertainties and almost two orders of magnitude below the data uncertainties. The degenerate-mass hypothesis is thus highly justified. We use the quick-Ly α option to convert gas particles with overdensities exceeding 10^3 and temperature below 10^5 K into stars. The simulations cover the volume of a periodic $100 \text{ Mpc}/h$ box, containing the equivalent of 3072^3 particles of each type. Following a method originally suggested in [37], we obtain this resolution by splicing together large-volume and high-resolution simulations, using a transition simulation that corrects the large-box simulation for its lack of coupling between small and large modes, and the high-resolution simulation for its small volume. We studied the accuracy of the splicing technique in [28] and [17], and we correct for residual biases by the nuisance parameters A^{splice} and η^{splice} . Snapshots are produced at regular intervals in redshift from $z=4.6$ to 2.2 , with $\Delta z=0.2$, thus corresponding to the same redshift bins as for the Lyman- α data.

¹<http://cosmo.nyu.edu/roman/2LPT/>

The dependence of the Lyman- α flux power spectrum on the parameters of interest is modeled by a Taylor expansion within a set of cosmological $\{\sigma_8, n_s, H_0, \Omega_m, \sum m_\nu$ or $1/m_X, \alpha_s\}$ and effective astrophysical $\{T_0(z=3), \gamma(z=3), A^\tau, \eta^\tau\}$ parameters. The grid of simulations required for this interpolation consists of a reference simulation centered on the Planck 2013 best-fit cosmology [38] and an IGM thermal history in agreement with [39, 40], completed by simulations where one or two parameters at a time are given off-centered values. These simulations are used to compute a full second-order Taylor expansion around the Lyman- α flux power spectrum measured for the reference case.

The cosmological parameters cover the range $H_0 = 67.5 \pm 5 \text{ km s}^{-1} \text{ Mpc}^{-1}$, $\Omega_M = 0.31 \pm 0.05$, $n_s = 0.96 \pm 0.05$, $\sigma_8 = 0.83 \pm 0.05$. In all the runs, we keep $\Omega_b = 0.0221$. To constrain neutrino masses, additional simulations are run with $\sum m_\nu = 0.4$ or 0.8 eV. Where WDM is assumed, the dark matter particles are thermal relics with masses $m_X = 2.5$ or 5.0 keV. Since Λ CDM is reproduced for $m_X \rightarrow \infty$, we use $1/m_X$ instead of m_X in the Taylor expansion, and the simulations therefore probe $1 \text{ keV}/m_X = 0, 0.2$ and 0.4 . When running of the scalar index is assumed, we use a set of simulations where the running parameter $\alpha_s \equiv dn_s/d \ln k$ is fixed to ± 0.04 . This allows us to introduce running directly in the Taylor expansion and thus fully account for its impact on the 1D Lyman- α flux power spectrum, whether direct or through cross-correlations with the other parameters. This feature was not included in the previous analysis of PY15 [17], where running was included a posteriori through a change of n_s between large (CMB) and small (Lyman- α) scales according to the relation $n_s(k) = n_s(k_p) + \alpha_s \times \ln(k/k_p)$.

Astrophysical parameters are varied in the simulations by modifying the UV background. The photoheating rates are varied to cover the range $\gamma(z=3) = 1.3 \pm 0.3$ and $T_0(z=3) = 14000 \pm 7000 \text{ K}$ in the outputs, where the IGM temperature is modeled for each redshift according to the usual relation $T = T_0 \times (\rho/\langle\rho\rangle)^{\gamma-1}$ [41]. The photo-ionization rate of each simulation was fixed by requiring the effective optical depth at each redshift to follow the empirical law $\tau_{\text{eff}}(z) = A^\tau (1+z)^{\eta^\tau}$, with $A^\tau = 0.0025 \pm 0.0020$ and $\eta^\tau = 3.7 \pm 0.4$ in agreement with [39], and where $\tau_{\text{eff}}(z)$ is defined with respect to the mean flux as $\tau_{\text{eff}}(z) \equiv -\ln\langle F(z)\rangle$. This renormalization was done at the post-processing stage, as justified in [42], allowing us to model the impact of different scalings without running new simulations.

The full modeling of the Lyman- α flux power spectrum includes further parameters to allow for additional freedom in the IGM thermal history and to account for remaining uncertainties or biases. We thus allow $T_0(z)$ and $\gamma(z)$ to vary as $(1+z)^\eta$, with a broken power law at $z=3$ for T_0 and a single power law for γ , as done in several previous works and in agreement with the recent works of [43, 44]. We also include two amplitudes for the correlated absorptions by Lyman- α with Si II and Si III, which we use as multiplicative corrections to the flux power spectrum. The study of WDM requires one to be able to lift the degeneracy between Jeans smoothing and WDM free streaming. Therefore, for WDM studies, we account for changes in the redshift of reionization by adding a nuisance term that reproduces the impact of z_{reio} on the redshift and mode dependence of the flux power spectrum, as was done in [10]. The remaining parameters are nuisance parameters that allow us to account for uncertainties or corrections related to noise in the data, spectrograph resolution, bias from the splicing technique, UV fluctuations in the IGM, residual contamination from unmasked DLA, and supernova and AGN feedbacks. Details on the fit parameters and on the dependence with scale and redshift of the nuisance parameters can be found in PY15 [17]. In this work

we introduce an improved modeling of the AGN feedbacks derived from the detailed study of [45]. The authors measure a significant and well understood impact of AGN feedback on the Lyman- α forest properties, which suppresses the Lyman- α 1D flux power spectrum by up to 6% on large scales, and of order 1% on the smallest scales probed by the eBOSS data. The SN feedback acts on similar scales, and partially compensates the effect of AGNs. We adopt the new more accurate model from [45] to correct the predicted power spectrum for the AGN feedback and we use the same study as before from [46] to correct for the SN feedback. For both feedbacks, we apply a Gaussian prior around the central value of the correction (see table 2). The definition of all parameters that describe the Lyman- α flux power spectrum can be found in table 1.

2.3 Interpretation methodology

To assess the robustness of the results, we use two different interpretation methodologies; frequentist and Bayesian. We briefly explain below how we combine the Lyman- α and CMB studies in both cases.

2.3.1 Frequentist interpretation

Our determination of the coverage intervals of unknown cosmological parameters is based on the “classical” confidence level method originally defined by [47]. We start with the likelihood $\mathcal{L}(x, \sigma_x; \Theta)$, for a given cosmological model defined by the n cosmological, astrophysical and nuisance parameters $\Theta = (\theta_1, \dots, \theta_n)$, and for data measurements x with Gaussian experimental errors σ_x . In the rest of this paper, we adopt a χ^2 notation, which means that the following quantity is minimized:

$$\chi^2(x, \sigma_x; \Theta) = -2 \ln(\mathcal{L}(x, \sigma_x; \Theta)) . \quad (2.1)$$

We first determine the minimum χ_{\min}^2 of $\chi^2(x, \sigma_x; \Theta)$ leaving all the cosmological parameters free. Then, to set a confidence level (CL) on any individual cosmological parameter θ_i , we scan the variable θ_i : for each fixed value of θ_i , we minimize again $\chi^2(x, \sigma_x; \Theta)$ but with $n - 1$ free parameters. The χ^2 difference, $\Delta\chi^2(\theta_i)$, between the new minimum and χ_{\min}^2 , allows us to compute the CL on the variable, assuming that the experimental errors are Gaussian,

$$\text{CL}(\theta_i) = 1 - \int_{\Delta\chi^2(\theta_i)}^{\infty} f_{\chi^2}(t; N_{dof}) dt , \quad (2.2)$$

with the χ^2 distribution

$$f_{\chi^2}(t; N_{dof}) = \frac{e^{-t/2} t^{N_{dof}/2-1}}{\sqrt{2^{N_{dof}} \Gamma(N_{dof}/2)}} , \quad (2.3)$$

where Γ is the Gamma function and the number of degrees of freedom N_{dof} is equal to 1. This profiling method can be easily extended to two variables. In this case, the minimizations are performed for $n - 2$ free parameters and the confidence level $\text{CL}(\theta_i, \theta_j)$ is derived from Equation (2.2) with $N_{dof} = 2$.

In this paper we also combine the χ^2 derived from the Ly α likelihood with that of Planck. In the frequentist analysis, we do not use the Planck likelihoods directly, but we

Parameter	Minimum	Maximum	Gaussian Mean	Gaussian Sigma
f_{SiIII}	-0.2	0.2	-	-
f_{SiII}	-2.0	2.0	-	-
A^{τ}	0	1.5	-	-
η^{τ}	0	7.0	-	-
$T_0(z=3)$	0	25000	-	-
$\gamma(z=3)$	0.3	2.0	1.3	0.3
$\eta^T(z < 3)$	-5.0	2.0	1.0	2.0
$\eta^T(z > 3)$	-10.0	2.0	-2.0	3.0
η^{γ}	-5.0	2.0	0.1	1.0
z_{reio}	7.0	15.0	-	-
A^{splice}	-1.0	1.0	0.01	0.05
η^{splice}	-40.0	40.0	0	2.5
A^{SN}	0.0	3.0	1.0	0.3
A^{AGN}	0.0	3.0	1.0	0.3
A^{UVfluct}	0.0	3.0	0	0.3
$A^{n,i}$	-2.0	2.0	0	0.02

Table 2. Bayesian prior ranges on astrophysical/nuisance parameters. The priors are either flat (denoted with - signs), or Gaussian with given mean and standard deviation. The z_{reio} parameter is only used for the thermal warm dark matter case.

use the Markov chains available in the official Planck² repositories instead. For instance, for the Planck 2018 TT+TE+EE configuration with massive neutrino, we take the chains from the directory `base_mnu/plikHM_TTTEEE_lowl_lowE`, which we reduce to the cosmological parameters $\{\sigma_8, n_s, \Omega_m, H_0, \sum m_\nu\}$ that are relevant for our analysis. The distribution of the chain elements allow us to estimate the posterior probability distributions for each parameter and the correlations between parameters. The flat positive prior applied to $\sum m_\nu$ causes a distortion of all posterior probability distributions, in particular for $\sum m_\nu$, and thus also for $\{\sigma_8, \Omega_m\}$, which are strongly correlated with $\sum m_\nu$. The posterior probability distribution becomes asymmetric and cannot be modeled by a simple Gaussian distribution. To account for such effects, we first apply a Principal Component Analysis on the reduced chain that allows us to determine the linearly uncorrelated variables, called the principal components. We then model the distribution of each principal component by several asymmetric Gaussians. We validated this strategy for a few configurations by comparing the limits obtained on $\sum m_\nu$ with this modeling with the limits derived directly from the MCMC approach using the full likelihood. The agreement between the two approaches was typically at the level of a few percent.

2.3.2 Bayesian interpretation

The Bayesian determination of the credible intervals of the parameters is based on their full posterior distribution according to Bayes theorem. The posterior distribution represents the probability distribution of the estimation of the true parameter value, which was improved upon by the experiment compared to the prior estimation. To obtain the posterior distribution, we use the implementation of the Metropolis Hastings algorithm from

²https://wiki.cosmos.esa.int/planck-legacy-archive/index.php/Cosmological_Parameters

MONTEPYTHON 3 [48] for our Monte-Carlo Markov Chains (MCMC). For each case, we run chains of an average total length of around 7 million steps, out of which on average around 1.5 million steps are accepted. We have explicitly checked that the convergence criteria of Gelman-Rubin for any parameter of any run are at most $|R - 1| < 0.01$.

For our cosmological parameter basis we choose $\{\omega_b, \omega_{\text{cdm}}, 100\theta_s, \ln 10^{10} A_s, n_s, \tau_{\text{reio}}\}$, plus a total neutrino mass $\sum m_\nu$ split between three degenerate species. Since this corresponds to the parameter basis in the Planck analysis, one can directly see the improvement coming from the addition of Lyman- α data. Many of the common degeneracies in CMB data analyses are removed by choosing appropriate flat priors (e.g. on θ_s instead of H_0). However, we checked explicitly (e.g. with runs assuming a flat prior on H_0 rather than θ_s , σ_8 rather than $\ln 10^{10} A_s$, and Ω_m rather than ω_{cdm}) that the choice of the parameter basis does not significantly influence the results.

The prior range for each astrophysical or nuisance parameter is shown in table 2. Cosmological parameters are all allowed to vary freely without bounds (which amounts to assuming a flat prior in a wide range compared to the width of the posterior), except for two cases. We impose $\tau_{\text{reio}} > 0.004$, since smaller values imply a reionization happening below redshift $z = 1$, which causes numerical problems and is now excluded by almost all data sets. Additionally, we impose the physical limitation $\sum m_\nu > 0$. Note that oscillation experiments constrain $\sum m_\nu$ to be larger than at least $\sqrt{|\Delta m_{32}^2|} \sim 0.05\text{eV}$ (see e.g. [49], section 14). Assuming a lower prior edge $\sum m_\nu > 0$ still makes sense: it amounts to studying limits on neutrino masses with minimal assumptions on neutrino decoupling and neutrino stability on cosmological time scales (which is not granted, e.g. [50, 51]). One could adopt a different point of view and derive cosmological bounds under the assumption that neutrinos decouple in the standard way and are fully stable, such that the oscillation prior $\sum m_\nu > 0.05\text{eV}$ applies. This would lead to slightly weaker cosmological bounds on $\sum m_\nu$ [52]. Both approaches are consistent but simply address different questions. In this work, we only explore the first prior choice.

The 95% CL for the sum of the neutrino masses is always derived as containing 95% of the full posterior integral, starting from the lower bound of the posterior. The quoted 1σ uncertainties on the other parameters are those that contain $\sim 68.3\%$ of the posterior centered around the mean value. Usually the 1D posteriors are close enough to being Gaussian that we do not display information other than the mean and sigma values.

3 Results

We present below the results obtained with both methodologies. We first focus on the constraints from Lyman- α data alone, and assess their compatibility with CMB constraints. In particular, we discuss a mild tension in the Ω_m parameter between the CMB and Lyman- α data. We then combine the data sets, assuming either a minimal cosmology (Λ CDM with massive neutrinos) or some basic extensions that may reduce this mild tension, with a particular focus on models with a running of the primordial spectral index. We discuss active neutrino mass bounds and their robustness against different assumptions. Finally, we present the constraints obtained for warm dark matter in the form of a thermal relic of mass m_X or in the form of a non-resonantly-produced sterile neutrino of mass m_s , which are robust with respect to the aforementioned tension.

	Frequentist		Bayesian	
	$m_\nu = 0$	Varying m_ν	$m_\nu = 0$	Varying m_ν
T_0 ($z=3$) (10^3K)	8.5 ± 1.9	8.5 ± 2.0	8.6 ± 1.9	8.6 ± 1.9
γ	0.93 ± 0.14	0.93 ± 0.14	0.96 ± 0.15	0.98 ± 0.14
σ_8	0.826 ± 0.020	0.826 ± 0.021	0.823 ± 0.022	0.811 ± 0.024
n_s	0.954 ± 0.006	0.954 ± 0.006	0.953 ± 0.007	0.955 ± 0.007
Ω_m	0.269 ± 0.009	0.269 ± 0.009	0.270 ± 0.010	0.275 ± 0.012
$\sum m_\nu$ (eV , 95% CL)	-	< 0.58	-	< 0.71

Table 3. Preferred astrophysical and cosmological parameter values (68.3% confidence level) for the $\Lambda\text{CDM} + m_\nu$ model, for Lyman- α data combined with a Gaussian prior $H_0 = 67.3 \pm 1.0 \text{ km s}^{-1} \text{ Mpc}^{-1}$.

3.1 Cosmological constraints from Lyman- α data alone

As was noted in PY15 [17], the Lyman- α forest flux power spectrum only weakly depends on the Hubble parameter, and is unable to constrain H_0 by itself. When using Lyman- α data alone, we thus adopt the same Gaussian prior constraint as in [10, 11, 20, 28], which is taken from the Planck 2015 TT+lowP results [53], namely $H_0 = 67.3 \pm 1.0 \text{ km s}^{-1} \text{ Mpc}^{-1}$. Note that most recent result from [54] using TT, TE, EE, low E + lensing gives $H_0 = 67.36 \pm 0.54$, in perfect agreement with the prior mentioned above. In [28], we explicitly checked that bounds on other parameters depend very weakly on the choice of H_0 prior. In particular, the Lyman- α posteriors are *not* significantly different when we combined the Lyman- α data with an H_0 prior taken from the SH₀ES results [55].

The IGM thermal history is one of the main sources of nuisance in this study. To encompass a large range of possible histories, we marginalize over the thermal parameters of table 1 to derive constraints either on $\sum m_\nu$ (sections 3.1 to 3.5) or on the mass of a WDM thermal relic (section 3.6). We show in appendix A the recovered best-fit thermal history in each case. Because of the freedom allowed in the modeling, the uncertainties on the thermal parameters are large, and the 2σ range on T_0 , γ and mean flux overlaps with observational measurements. To further test the robustness of our result, we also investigate how the constraints we derive depend on our hypotheses and we investigate the impact of a different thermal model. As shown in appendix A, imposing a thermal model in agreement with a specific set of measurements [40] has little impact on the measured bounds.

As a sanity check on the interpretation methodologies, we assess the compatibility between the Bayesian and frequentist best-fit values of the cosmological parameters for Lyman- α data alone, in the standard ΛCDM cosmological model with massless or massive neutrinos. As shown in table 3, the results for the two methodologies are in excellent agreement, both for the central value of the parameters and for their uncertainty. The flux power spectrum of the best-fit model is shown in figure 1. Compared to the previous work of PY15 [17], there is a noticeable improvement in the agreement between the data and the best-fit model, in particular for high k and high z .

The best fit on Lyman- α data alone slightly differs from the one obtained on the DR9 data for two cosmological parameters: n_s , which increased from 0.938 ± 0.010 in PY15 [17] to

0.954 ± 0.006 , and Ω_m , which decreased from 0.293 ± 0.014 to 0.269 ± 0.009 . We investigated the origin of this $\sim 1.5\sigma$ shift. Restricting the eBOSS data to the forests in common with those from DR9, we measure $n_s = 0.945 \pm 0.008$ and $\Omega_m = 0.278 \pm 0.015$. To further mimic the DR9 selection, we then replace the automated catalogs of Broad Absorption Line quasars and Damped Lyman- α systems by the visual catalogs that were used in DR9. The fit on the resulting sample gives $n_s = 0.935 \pm 0.008$ and $\Omega_m = 0.282 \pm 0.015$, in good agreement with the cosmology obtained with the analysis of PY15 [17] on the DR9 sample. This result concurs with what was found in a similar study led in [20]. The change in the data is therefore at the origin of the small shift in best-fit cosmological parameters.

3.2 Mild tension between Planck and Lyman- α data

Before combining the Lyman- α data with CMB data, we compare the results from the Lyman- α DR14 flux power spectrum (see table 3) and from Planck 2018 (see table 4) with minimal assumptions on the cosmological model, i.e. in the framework of the Λ CDM ν model with a free value of $\sum m_\nu$. The common free parameters in the Lyman- α and Planck likelihoods are the primordial spectrum amplitude and spectral index $\{\sigma_8 \text{ or } A_s, n_s, \}$, the fractional density of matter Ω_m , and possibly the neutrino mass $\sum m_\nu$. There are two more common parameters Ω_b and H_0 , but the Lyman- α data are so weakly sensitive to them that we fixed Ω_b and imposed an H_0 prior that guarantees agreement with Planck.

For all common parameters but one, we find excellent agreement between the confidence bounds derived from Lyman- α data and CMB data. This can be checked directly from tables 3 and 4, or visually by comparing two-dimensional contours in the $\{\sum m_\nu, \sigma_8, n_s\}$ plane in figures 2 and 3. In the Bayesian case, one should look at figure 2 and compare red contours (Lyman- α) with blue contours (P18+lens+BAO). In the frequentist case, figure 3 shows again the Lyman- α contours in red and the P18 contours in blue. For instance, for n_s , the Lyman- α and P18+lens+BAO bounds are compatible at the 1.4σ level.

We find a mild tension between the Ω_m values derived from CMB data ($\Omega_m \sim 0.31$) and Lyman- α data ($\Omega_m \sim 0.27$). The tension is present with both methodologies, with or without massive neutrinos, and with respect to both the P18 and P18+lens+BAO datasets. For instance, in the Λ CDM ν model, the Bayesian (resp. frequentist) analysis returns a 2.5σ (resp. 3.6σ) tension between the Ω_m values derived from the BOSS DR14 flux spectrum and the P18+Lens+BAO combination. This tension is displayed in the $\{\Omega_m, n_s\}$ plane in the left panel of figure 4.

Figure 4 (left panel) shows that for a fixed value of Ω_m around 0.31, this mismatch could instead be interpreted as a mild tension on n_s . This is reminiscent of a similar tension on n_s found with previous Lyman- α data from BOSS DR9 discussed in [17]. When fitting the parameters of the Λ CDM model or its extensions to Lyman- α data, n_s and Ω_m are always anti-correlated, because they both affect the overall slope of the flux power spectrum in the same direction. Therefore the tension on Ω_m in the present version of the data set and likelihood is likely to have the same origin as the tension on n_s in the previous version: whether the tension is interpreted as one on n_s or as one on Ω_m strongly depends on the modeling of the data and its systematics. In any case, since the analysis presented in this work is based on the most up-to-date data set and on the most advanced systematic modeling

	P18	P18 + lens. +BAO
σ_8	0.804 ± 0.018	0.815 ± 0.009
n_s	0.9630 ± 0.0048	0.966 ± 0.004
Ω_m	0.321 ± 0.014	0.310 ± 0.007
$100\Omega_b$	2.232 ± 0.016	2.241 ± 0.014
H_0 (km s ⁻¹ Mpc ⁻¹)	66.9 ± 1.1	67.81 ± 0.5
$\sum m_\nu$ (eV , 95% CL)	< 0.286	< 0.113

Table 4. Preferred cosmological parameter values (68.3% confidence level) for the Λ CDM + $\sum m_\nu$ model, for Planck data alone or combined with BAO data, as extracted from Bayesian chains containing ~ 6.5 million points. The convergence criterion of the chains is $|R - 1| < 10^{-3}$ for all parameters, such that these chains are slightly more converged than the publicly available ones.

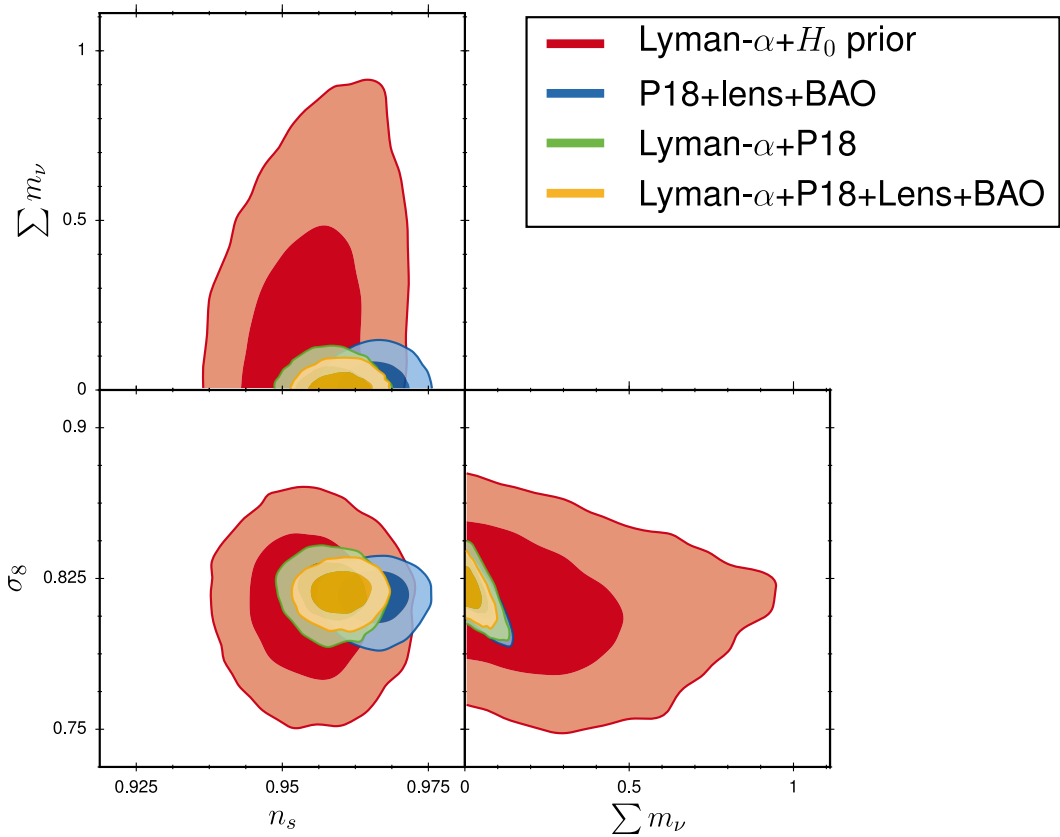


Figure 2. Bayesian marginalized 2D posteriors in the sub-space $\{\sum m_\nu, \sigma_8, n_s\}$ for the Λ CDM ν model and various combinations of CMB, BAO and Lyman- α data. We show the 68.3% (1σ) and 95.4% (2σ) limits.

of the BOSS and eBOSS flux power spectrum, we will concentrate on the Ω_m tension and its possible origins.

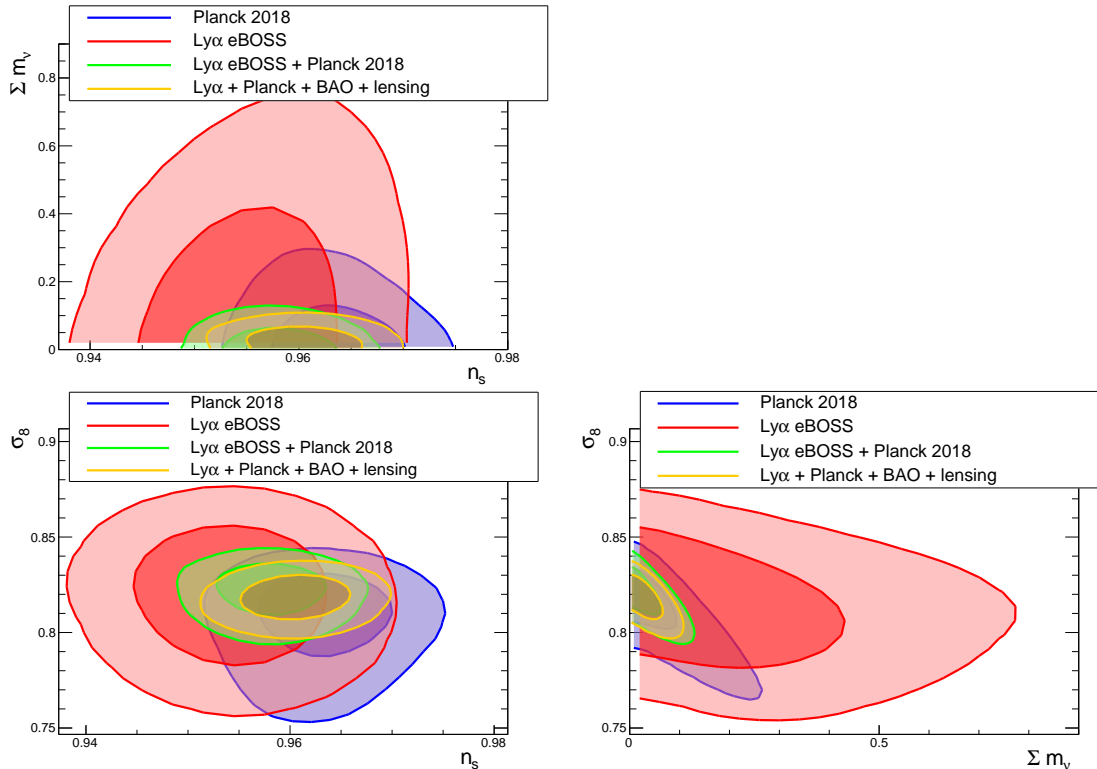


Figure 3. Frequentist 2D isocontours in the sub-space $\{m_{\text{tot}} = \sum m_\nu, \sigma_8, n_s\}$ for the $\Lambda\text{CDM}\nu$ model and various combinations of CMB, BAO and Lyman- α data. We show the 68% and 95% contours.

We stress that the Lyman- α results are nicely consistent with those from weak lensing (WL) surveys. Over the past years, there has been a mild but persistent tension between likelihood contours in the (Ω_m, σ_8) plane inferred from Planck data and from WL surveys, when assuming either a ΛCDM or $\Lambda\text{CDM}\nu$ cosmology. This is commonly referred to as the “ σ_8 tension”, although Ω_m is also involved. The tension is actually best seen when quoting results on the combination $S_8 \equiv \sigma_8(\Omega_m/0.3)^{0.5}$ which is orthogonal to a direction of degeneracy in the WL posteriors.

In Figure 5, we show the contours of the new BOSS + eBOSS DR14 Lyman- α data (combined again with a H_0 prior) in the (Ω_m, σ_8) and (Ω_m, S_8) planes, compared with those from one of the most recent joint analyses [56] of several WL data sets (DES-Y1 [60, 61], KV450 [62]), and finally compared with Planck contours, assuming in each case a ΛCDM cosmology. The left panel of Figure 5 shows that the σ_8 tension can be equally well interpreted as an Ω_m tension. While the CMB versus WL tension is strongest in the S_8 direction, the CMB versus Lyman- α tension is strongest in the Ω_m direction. It is striking to see that WL and Lyman- α data, which are two late time probes of a similar range of scales, agree with

⁴Instead of using the DES-Y1 redshift distributions [57], these new analyses use photometric redshifts from COSMOS-2015 [56, 58, 59]. Note also that we are considering a flat ΛCDM model in agreement with the cited analyses.

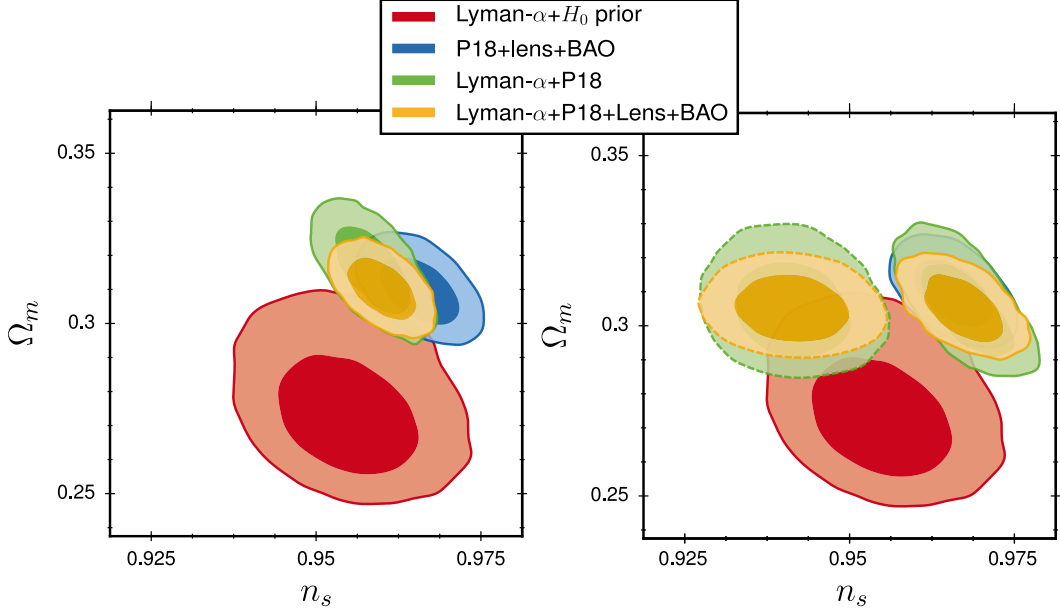


Figure 4. Bayesian marginalized 2D posteriors in the sub-space $\{\Omega_m, n_s\}$ assuming various cosmological models and combinations of CMB, BAO and Lyman- α data. We show the 68.3%(1σ) and 95.4%(2σ) limits. **Left:** Λ CDM ν model, showing a mild tension. **Right:** Λ CDM ν model with two independent tilts for the Planck and Lyman- α likelihoods.

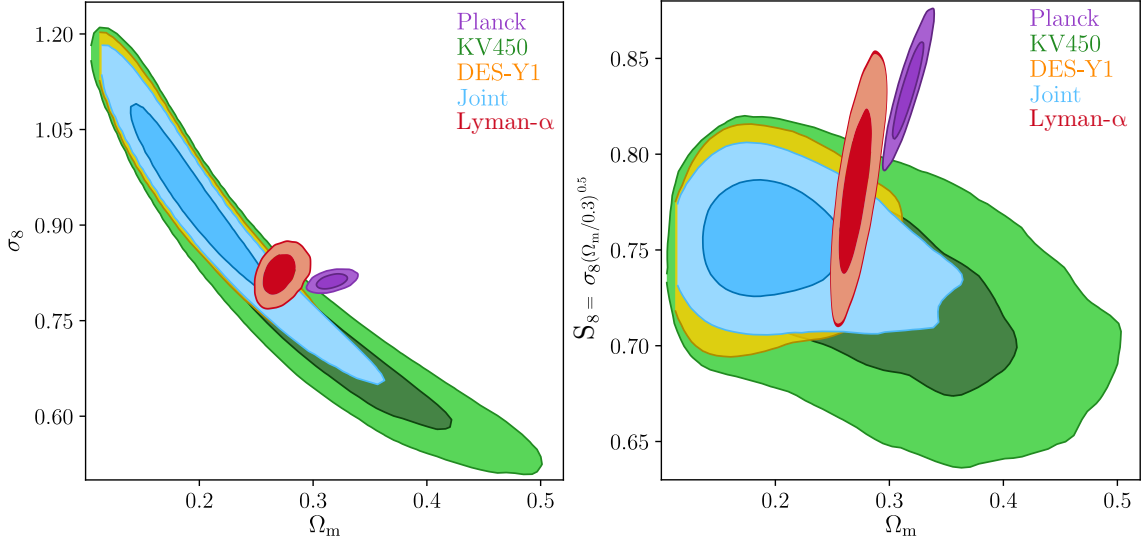


Figure 5. Comparison of the $\{\sigma_8, \Omega_m\}$ and $\{S_8, \Omega_m\}$ planes for Planck, Weak Lensing surveys (DES, KiDS+VIKING), and Lyman- α data, where $S_8 \equiv \sigma_8 (\Omega_m/0.3)^{0.5}$. The tension between Lyman- α and CMB data is here best described as a tension in Ω_m . The COSEBI-based redshift-recalibrated analyses for DES-Y1⁴, KV450, and their joint constraint are taken from Asgari et al. [56].

each other at the 1σ level, while they are both in tension with the Planck best-fit Λ CDM model at the 2.5σ to 3.6σ level.

Configuration	$\Delta\chi^2$	Configuration	$\Delta\chi^2$
$0.0010 < k < 0.017$	-0.2	DLA model (Rogers)	0.0
$0.0025 < k < 0.020$	-4.3	Alternative splicing (1)	-2.1
$2.1 < z < 4.5$	+2.4	Alternative splicing (2)	-0.6
$2.1 < z < 4.3$	+8.4	Top hat prior on H_0	+5.8
$2.3 < z < 4.7$	+3.4	Two independent n_s	-13.8
$2.5 < z < 4.7$	+2.5	Running of n_s	-8.2

Table 5. Tests performed to investigate possible sources of improvement of the consistency between Lyman- α and Planck likelihoods. Improvement is quantified by $\Delta\chi^2$: the χ^2 difference between separate and combined data sets.

We performed a systematic search of the origin of this tension, investigating possible sources of systematics both at the level of the modeling of the Lyman- α 1D flux power spectrum and at the level of the Lyman- α data analysis. In table 5, we summarize in each case the improvement in the consistency of the Lyman- α and the CMB likelihoods, which we quantify by the change in the χ^2 difference between separate and combined data sets. A negative $\Delta\chi^2$ indicates an improved agreement, whereas a positive $\Delta\chi^2$ shows an enhanced tension. We first considered sub-samples of the Lyman- α data to identify possible regions in k or in z -space that would pull the fit away from the model preferred by CMB data. The results are reported in the left column of table 5. We tested the impact of the smallest scales (cutting out $k > 0.017 \text{ s km}^{-1}$) as these are the most affected by our knowledge of the spectrograph resolution and our understanding of the noise power contribution (first row). We tested removing the large-scale modes (restricting to $k > 0.0025 \text{ s km}^{-1}$) instead, since these have the smallest statistical uncertainties and hence a large constraining power on the slope of the power spectrum (second row). We selected different redshift ranges, keeping only the lowest redshift bins (rows 3 and 4) that have better statistics, or instead the higher redshift ones (rows 5 and 6) that are less prone to systematics related to the measurement of the noise power. None of these tests yielded any significant change in the Lyman- α best-fit cosmological values.

In a second stage, we modified in several ways the model we use to fit the Lyman- α data (right column of table 5). The first test was using the correction suggested by [63] to account for the incompleteness of the masking of the damped Lyman- α systems (DLA) in the data, instead of the one from [64] that was used in [20]. This had no impact, as shown in the first row. As detailed in PY15 [17], the splicing technique produces a k -dependent bias caused by the change of splicing regime at a pre-determined pivot scale. The bias can be modeled by a broken line with a possible, albeit small, trend for some redshift evolution. We applied two new correction models to test whether the model we had opted for was responsible for the different slopes preferred by the Lyman- α and the CMB data. The model adopted in PY15 [17] includes a low- k slope and a redshift evolution that are taken from the splicing study, and two free parameters: the high- k slope and the offset at the pivot scale. Alternative splicing 1 is a model with no redshift dependence, a high- k slope fixed to 0 and two free parameters: the low- k slope and the offset. Alternative splicing 2 has no redshift dependence, but allows for variation in both low- k and high- k slopes as well as a free offset. Neither splicing model yields a notable change on $\Delta\chi^2$. Finally, we also tested fitting the Lyman- α

data with a loose flat prior on H_0 between 55 and 80 km s⁻¹ Mpc⁻¹, instead of the usual Gaussian prior of $H_0 = 67.3 \pm 1.0$ km s⁻¹ Mpc⁻¹. This had negligible impact on the result, as expected from the earlier studies of [28]. The last two lines of table 5, assuming two distinct values of n_s on large and small scales or a running of n_s , refer to the study we describe in detail in the next two sections, and which leads to a notable improvement on the agreement between Lyman- α and CMB data.

We cannot exclude the possibility that the tension between the value of Ω_m preferred by CMB and Lyman- α data originates from yet another unidentified systematics (or imperfection in the computation of the Lyman- α likelihood). Indeed, with statistical uncertainties on the data points down at the percent level, results on cosmological parameters are now hitting the systematics floor. Despite the great care that went into their modeling, instrumental features – such as correction of spectrograph resolution and subtraction of noise power – affect the lowest redshift bins and the smallest scales at a level comparable to the statistical uncertainties. Uncertainties also arise on the simulation side, mostly in relation to the use of the splicing technique mentioned above. Although the bias induced by this approach was measured to be small, and although we mitigate the risk of an imperfect modeling by marginalizing over the parameters that correct for the impact of splicing, a residual bias on the large-scale correction would affect the slope of the 1D flux power spectrum and could be responsible for the observed tension.

3.3 Combining CMB and Lyman- α data

CMB and Lyman- α data can be combined with different assumptions on the underlying cosmology.

First, one can adopt the point of view that the tension on Ω_m described in section 3.2 is sufficiently small that it should not prevent us from combining the data sets while sticking to the Λ CDM ν model. In this case, the combined limits on cosmological parameters – using either the frequentist or Bayesian methodology – are presented in table 6. We will come back to the discussion of the neutrino mass bounds found in this analysis in a dedicated section 3.5. Since the Planck data has more statistical weight, the Ω_m values in the combined fit are driven to Planck best-fit values, as shown in figure 4. The other cosmological parameters, already in good agreement between their best-fit values for the two data sets taken individually, do not change significantly. While Planck data carry no information per se on the IGM thermal history, they can affect the best-fit values of the astrophysical parameters through their correlations with the cosmological terms. For instance, the anti-correlation between Ω_m and γ – and to a lesser extent between n_s and γ – is causing γ to decrease compared to its value for the fit with Lyman- α data alone, since both Ω_m and n_s are increased. All correlation coefficients, and comments thereof, are provided in appendix B.

	Frequentist		Bayesian	
	P18 + Lyman- α	P18 + Lyman- α +lens. +BAO	P18 + Lyman- α	P18 + Lyman- α +lens. +BAO
T_0 (z=3) (10^3 K)	9.7 ± 1.7	9.8 ± 2.0	9.5 ± 1.8	9.5 ± 1.8
γ	0.69 ± 0.10	0.68 ± 0.11	0.71 ± 0.10	0.71 ± 0.10
σ_8	0.825 ± 0.006	0.819 ± 0.008	0.818 ± 0.010	0.818 ± 0.007
n_s	0.958 ± 0.003	0.961 ± 0.003	0.959 ± 0.004	0.960 ± 0.003
Ω_m	0.311 ± 0.006	0.308 ± 0.006	0.316 ± 0.009	0.310 ± 0.006
$\sum m_\nu$ (eV , 95% CL)	< 0.099	< 0.089	< 0.099	< 0.074

Table 6. Preferred astrophysical and cosmological parameter values (68.3% confidence level) for the Λ CDM + m_ν model, for combined Lyman- α , CMB and BAO data.

	Frequentist		Bayesian	
	P18 + Lyman- α	P18 + Lyman- α +lens. +BAO	P18 + Lyman- α	P18 + Lyman- α +lens. +BAO
T_0 (z=3) (10^3 K)	7.6 ± 1.9	7.6 ± 1.8	8.2 ± 1.6	8.2 ± 1.6
γ	0.88 ± 0.13	0.88 ± 0.08	0.90 ± 0.12	0.89 ± 0.12
σ_8	0.824 ± 0.008	0.820 ± 0.008	0.814 ± 0.010	0.818 ± 0.008
n_s (Planck)	0.965 ± 0.004	0.968 ± 0.004	0.968 ± 0.005	0.967 ± 0.004
n_s (Lyman- α)	0.942 ± 0.006	0.942 ± 0.005	0.941 ± 0.006	0.941 ± 0.006
Ω_m	0.304 ± 0.010	0.304 ± 0.006	0.305 ± 0.009	0.305 ± 0.006
$\sum m_\nu$ (eV , 95% CL)	< 0.126	< 0.104	< 0.109	< 0.087

Table 7. Preferred astrophysical and cosmological parameter values (68.3% confidence level) for the Λ CDM + m_ν model, for combined Lyman- α , CMB and BAO data, when introducing artificially two distinct n_s value in the Lyman- α and CMB likelihood.

	Frequentist		Bayesian	
	Lyman- α +P18	Lyman- α +P18 +lens. +BAO	Lyman- α +P18	Lyman- α +P18 +lens. +BAO
T_0 (z=3) (10^3 K)	7.8 ± 1.8	8.0 ± 1.8	8.5 ± 1.6	8.5 ± 1.6
γ	0.80 ± 0.12	0.80 ± 0.12	0.81 ± 0.11	0.80 ± 0.11
σ_8	0.825 ± 0.007	0.821 ± 0.007	0.817 ± 0.010	0.817 ± 0.008
n_s	0.962 ± 0.003	0.962 ± 0.003	0.962 ± 0.004	0.962 ± 0.004
Ω_m	0.306 ± 0.007	0.307 ± 0.006	0.310 ± 0.009	0.308 ± 0.006
α_s	-0.010 ± 0.003	-0.010 ± 0.003	-0.010 ± 0.004	-0.010 ± 0.004
$\sum m_\nu$ (eV , 95% CL)	< 0.105	< 0.089	< 0.101	< 0.088

Table 8. Preferred astrophysical and cosmological parameter values (68.3% confidence level) for the Λ CDM + m_ν + α_s model, for combined Lyman- α , CMB and BAO data.

Since for a fixed value of Ω_m around 0.31, the tension could be interpreted as a tension in n_s , it is interesting to check whether the two data sets can be brought in better agreement by allowing the overall slope of the CMB and Lyman- α flux power spectra to be independent of each other. To check this, we first perform an academic study in which we assume different values of n_s in the CMB and in the Lyman- α likelihoods. Our results for that case are presented in table 7.

In this configuration, the global χ^2 decreases by ~ 13.8 for P18+lens+BAO+Lyman- α compared to the Λ CDM ν fit, which represents an improved compatibility between Lyman- α and P18+lens+BAO and data. The corresponding two-dimensional $\{\Omega_m, n_s\}$ contours, displayed in the right panel of figure 4, now feature two distinct regions; one (dashed lines) for n_s (Lyman- α) and another (solid lines) for n_s (Planck). The two values of n_s are centered around $n_s = 0.967$ for Planck and $n_s = 0.941$ for Lyman- α data. In the right panel of figure 4, the improved compatibility shows up in the fact that the red contour (Lyman- α only) is now in better agreement with the green and yellow dashed contours (combined data set).

Of course, the improved agreement occurs at the price of rather unphysical assumptions. This exercise is however not completely artificial, because the CMB and Lyman- α data sets probe different fluctuations (photon perturbations or a tracer of baryons and CDM fluctuations) on different scales and at different times. Thus there could be many physical and sensible reasons for which the overall slope of the two observables are not correlated in the way predicted by the Λ CDM or Λ CDM ν models.

First, the primordial power spectrum could have a different effective slope $\frac{d \ln \mathcal{P}_{\mathcal{R}}}{d \ln k}$ due to physical mechanisms taking place during inflation. For instance, a large curvature in the inflaton potential could produce a running of the spectral index, i.e. a continuous variation of $\frac{d \ln \mathcal{P}_{\mathcal{R}}}{d \ln k}$ with k [65], while a kink in the potential could lead to a feature in the primordial spectrum with different spectral indices on large and small scale [66].

Second, the growth rate of dark matter could be reduced on small scales during radiation and/or matter domination, for instance due to small interactions between dark matter and other species or self-interactions in the dark matter sector, or by a small departure from Einstein gravity. Since baryons fall in the gravitational potential wells of dark matter, this reduction would propagate to the baryons and to the flux power spectrum. An example of a mechanism leading to a small reduction of the effective slope of the matter power spectrum $\frac{d \ln \mathcal{P}_m}{d \ln k}$ is provided by the scattering dark matter model of [67]. Another case is that of $f(R)$ gravity, that leads to a scale-dependent linear growth factor with less growth on small scales [68].

In principle, a dedicated analysis would be needed in order to investigate up to which extent each of these models can reduce the mild tension between Lyman- α and CMB data. In this work, we limit ourselves to the most studied among the previous models, featuring a running of the scalar index, $\alpha_s = \frac{d^2 \ln \mathcal{P}_{\mathcal{R}}}{d \ln k^2} = \frac{dn_s}{d \ln k}$, treated as constant over the range of scales probed by both CMB and Lyman- α data.

3.4 Λ CDM $\nu + \alpha_s$ cosmology

On the theoretical side, the running of the spectral index is usually connected to the physics of inflation, but we should keep in mind that it could be seen as an effective parametrization of

some of the other models described previously – in particular, a negative α_s gives a reduction of the amplitude and of the effective slope of the small-scale matter power spectrum that could mimic a scale-dependent reduction of the linear growth factor. The simplest inflationary models predict that the running of the spectral index should be of second order in inflationary slow-roll parameters and therefore small, $|\alpha_s| \sim (n_s - 1)^2 \sim 10^{-3}$ [65]. Nevertheless, it is possible to accommodate a larger scale dependence of n_s by adjusting the third derivative in the inflaton potential (see for instance [69, 70]).

On the experimental side, recent CMB experiments have a mixed history of null results and a-few-sigma detections of running of the scalar index. The final 9-year WMAP analysis found no evidence of running using WMAP alone, with $\alpha_s = -0.019 \pm 0.025$ at 68% CL, while the combination of WMAP data with the first data releases from ACT and SPT found a negative running at nearly the 2σ level with $\alpha_s = -0.022 \pm 0.012$ [71]. The ACT 3-year release measured $\alpha_s = -0.003 \pm 0.013$ when combining with WMAP-7 [72]. A negative running was detected at just over 2σ by SPT, $\alpha_s = -0.024 \pm 0.011$ [73]. The Planck 2018 results, while roughly consistent with zero running of the scalar spectral index, indicate a $\sim 1\sigma$ preference for negative running, $\alpha_s = -0.0041 \pm 0.0067$. Finally, in the paper PY15 [17], we reported a $\sim 3\sigma$ tension on n_s when we combined Planck 2015 and the DR9 BOSS Lyman- α measurement, which yielded $\alpha_s = -0.0117 \pm 0.0033$.

The analysis of PY15 [17], however, was simplified: the effect of running on the Lyman- α likelihood was approximated as a change in the spectral index following the relation $n_s(k) = n_s(k_p) + \alpha_s \times \ln(k/k_p)$. In the present work, we performed dedicated simulations accounting for the full effect of running on the primordial spectrum, and added α_s to the list of parameters in the Taylor expansion of the flux power spectrum and in the Lyman- α likelihood. The result of our combined fit of CMB and Lyman- α data for the Λ CDM $\nu + \alpha_s$ cosmology are presented in table 8. The value of the spectral index reported here is defined at the pivot scale $k_* = 0.05 \text{ Mpc}^{-1}$.

As in section 3.1, the Bayesian and frequentist approaches provide consistent results. Allowing a running of n_s improves the global fit to P18+lens+BAO+Lyman- α by $\Delta\chi^2 \sim 8.2$ compared to the plain Λ CDM ν model. This is a bit less than when floating two independent tilts, which yielded $\Delta\chi^2 \sim 13.8$. There are two reasons for this. First, the Lyman- α data alone shows no preference for negative running, i.e. for a negative curvature in the shape of the flux power spectrum. Thus, although the χ^2 of the combined fit decreases, the Lyman- α contribution to the total χ^2 increases slightly. Second, in the model with running, negative values of α_s also suppress the fluctuation amplitude on the smallest and largest scales probed by Planck (i.e., in the regions of the Sachs-Wolfe plateau and Silk damping tail). This disfavors too low values of the running, as shown by the Planck-only bound $\alpha_s = -0.0041 \pm 0.0067$. The fit with two independent n_s values does not have this effect on CMB data and allows for a slightly stronger variation of the spectrum slope between CMB and Lyman- α scales, explaining the stronger decrease in the best-fit χ^2 .

In a model with non-zero running, the Lyman- α data are compatible with significantly larger values of Ω_m than in the Λ CDM ν model. With a large negative running, the effective slope of the spectrum on Lyman- α scales can be small (corresponding to a small effective $n_s(\text{Lyman-}\alpha)$), and thus Ω_m can be large. We obtain a detection of running at the $\sim 3\sigma$ level. With both P18+Lyman- α and P18+Lyman- α +lensing+BAO data sets, we find $\alpha_s = -0.010 \pm 0.004$, in agreement with the previous measurement of PY15.

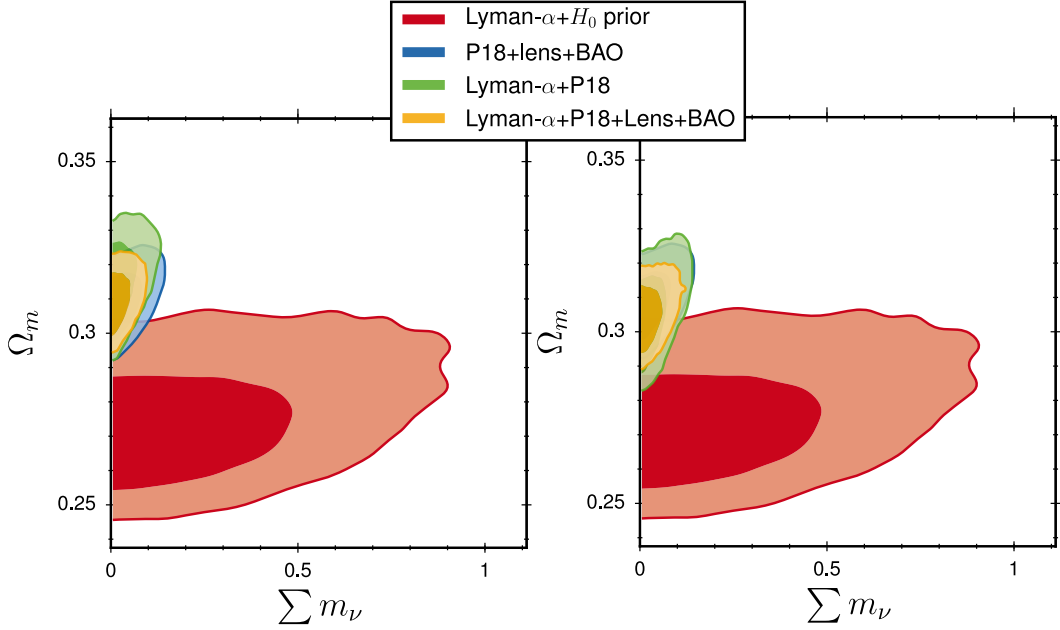


Figure 6. Bayesian marginalized 2D posteriors in the sub-space $\{\sum m_\nu, \Omega_m\}$ assuming various cosmological models and combinations of CMB, BAO and Lyman- α data. We show the 68.3%(1 σ) and 95.4%(2 σ) limits. **Left:** Λ CDM ν model, showing a mild tension. **Right:** Λ CDM ν model with two independent tilts in the Planck and Lyman- α likelihoods.

3.5 Neutrino mass bounds

The combination of Lyman- α and CMB data presents several advantages. CMB data alone is more sensitive to $\sum m_\nu$ than Lyman- α data alone, through CMB lensing, the integrated Sachs Wolfe effect, and the measurement of the angular diameter distance to recombination [74–76]. Combining the data sets helps in breaking degeneracies between cosmological parameters, such as between $\sum m_\nu$ and σ_8 (or A_s), n_s and Ω_m . This contributes to further tightening the constraint on $\sum m_\nu$.

The constraint on $\sum m_\nu$ coming from Lyman- α alone (with the H_0 prior) are included in table 3, and those from P18 or P18+lens+BAO in table 4. The joint bounds are presented in table 6 for the Λ CDM ν model, table 7 for the case with two independent spectral indices, and table 8 for the Λ CDM $\nu + \alpha_s$ case.

The joint Lyman- α +P18+lens+BAO on $\sum m_\nu$ are loosened by a moderate amount (16%) when switching from the Λ CDM ν fit (frequentist bound of 0.89 meV at 95%CL) to the fit with two free spectral indices (frequentist bound of 0.104 meV). To understand this, we can look at 2D contours in the $(\Omega_m, \sum m_\nu)$ space for these two models, shown in figure 6. The combined bounds are strongly influenced by the fact that Lyman- α data remove a degeneracy between Ω_m and $\sum m_\nu$ in the CMB+BAO data. Thus the neutrino mass bounds must be discussed together with the mild $\sim 2\sigma$ tension between the values of Ω_m preferred by the two data sets. Since the tension is the strongest in the Λ CDM ν model, the neutrino mass is the most constrained in this case. In the model with two spectral indices, the Lyman- α data accommodate slightly larger values of Ω_m , because they are partly compensated by lower

values of n_s at the level of the flux power spectrum. Thus the tension is relaxed and the neutrino mass bound gets a bit looser. The same trend is true in the $\Lambda\text{CDM}\nu + \alpha_s$ case, but the neutrino mass bounds remain slightly tighter than in the case with the two n_s values.

It is remarkable that all the neutrino mass bounds presented here fall within 20% of each other, despite the very different assumptions on the scale dependence of the spectral index. Our results for $\sum m_\nu$ are thus found to be robust against various assumptions on the possible origin of the mild tension between Lyman- α and Planck data when assuming a $\Lambda\text{CDM}\nu$ cosmology. As a final result for neutrino masses, we choose to highlight the bounds coming from the most conservative of our two analyses based on a physical model, namely, the $\Lambda\text{CDM}\nu + \alpha_s$ analysis. We obtain $\sum m_\nu < 0.11\text{eV}$ (resp. $< 0.09\text{eV}$) at the 95% confidence level for Lyman- α + P18 (resp. Lyman- α + P18+lens. +BAO) data, both from the frequentist or the Bayesian approach.

Given the results on neutrino oscillations (e.g. [77] for a review), these results put marginal tension on the inverted neutrino mass hierarchy scenario, which predicts a lower bound of 99.5 meV for $\sum m_\nu$. Note however that an analysis adopting the ‘‘oscillation prior’’ $\sum m_\nu > 0.05$ meV would return a looser bound than our analysis assuming $\sum m_\nu > 0$. Thus, inverted hierarchy cannot be considered as disfavored at the 2σ level by our data set.

We also explored the impact of higher-resolution Lyman- α data by including the XQ-100 flux power spectrum measured by [19]. The fit to the extended Lyman- α data set improves our sensitivity to neutrino masses, with tighter 3σ bounds and steeper likelihood profiles than in the case of DR14 Lyman- α data alone. However, XQ-100 has a very marginal preference for a non-zero neutrino mass, $\sum m_\nu = 0.13 \pm 0.18$ eV. Thus the combined bounds from Lyman- α XQ-100 + DR14 data (including the H_0 prior) are not stronger than from DR14 data alone as one may have expected: we find $\sum m_\nu < 0.53$ eV for the joint bound. This trend was already noticed in [19], and shown for instance in their figure 10. The same is true when CMB data is added on top. The limit obtained from DR14 + XQ-100 + P18 data assuming a $\Lambda\text{CDM}\nu$ cosmology, $\sum m_\nu < 0.122$ eV, is slightly degraded compared to the one shown in table 6, again in agreement with the study of [19].

3.6 Constraints on ΛWDM model

As explained in section 2.2, the simulation grid can also be used to derive constraints on warm dark matter (WDM) in the form of thermal relics, since we performed simulations with non zero values of $1\text{keV}/m_X$. Here, we use the set of WDM simulations presented in [10] to provide results on thermal relics and non-resonantly-produced (hereafter ‘‘NRP’’) sterile neutrinos. We refer to [10] for extensive justification of this approach and we only summarize the main result here.

As described by Dodelson and Widrow [78], a sterile neutrino population can be produced by non-resonant oscillations with the active sector in the early Universe (around $T \sim 100\text{MeV}$ for keV masses). This leads to a quasi-thermal distribution function for the sterile neutrinos, even if they never reached thermal equilibrium. Thanks to a symmetry in the evolution equations of linear perturbations, thermal WDM relics with a mass m_X produce the same cut-off in the linear power spectrum as NRP sterile neutrinos with a mass m_s inferred from

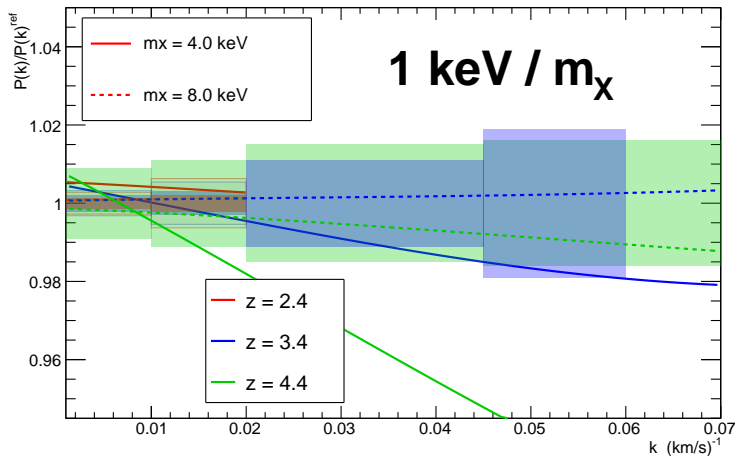


Figure 7. Sensitivity of the eBOSS and XQ-100 data to WDM. The curves show the predicted deviation of the Lyman- α flux power spectrum for a WDM particle mass of 4.0 keV (solid) or 8.0 keV (dashed) relative to Λ CDM, in three redshift bins, when all other cosmological, astrophysical and nuisance parameters are kept fixed. The boxes illustrate the data uncertainty using the same code as for the curves. The $z=2.4$ bin only refers to eBOSS data and is bounded to $k < 0.02 \text{ s km}^{-1}$. Shaded boxes refer to statistical errors only, while larger clear boxes bounded by colored lines refer to statistical plus systematic errors. Systematics only significantly impact the total uncertainty for $k < 0.02 \text{ s km}^{-1}$ (eBOSS data) and at small redshift ($z < 3.4$ typically).

the rescaling relation

$$\frac{m_s}{3.90 \text{ keV}} = \left(\frac{m_X}{\text{keV}}\right)^{1.294} \left(\frac{0.25 \times 0.7^2}{\Omega_{WDM} h^2}\right)^{1/3}. \quad (3.1)$$

Since for this category of models, WDM simulations depend on the nature of WDM only through the input linear power spectrum [79], simulations with thermal relics can also be used to derive bounds on NRP sterile neutrinos. Other classes, such as resonantly-produced sterile neutrinos, are of particular relevance. One cannot, however, constrain their mass through a simple rescaling of m_X . It requires a dedicated study that is beyond the scope of this work.

To constrain the mass of a WDM thermal relic, we use a Lyman- α data set consisting of the eBOSS DR14 data combined with the XQ-100 data from [19]. The use of high-resolution data to constrain WDM has recently been subject to debate [80, 81]. On the one hand, they are expected to be more sensitive to WDM as they better probe the scale range impacted by the WDM power suppression, as illustrated in Figure 7. On the other hand, this cut-off is partially degenerate with a similar effect caused instead by a warm IGM. We here use the same model of the IGM thermal history as in the previous sections, allowing, in addition, variations of z_{reio} as explained in section 2.2.

The eBOSS DR14 + XQ-100 Lyman- α data constrain the WDM mass to $m_X > 8.6 \text{ keV}$ (95% CL). Because non-linear structure growth tends to erase the power suppression caused by the free-streaming of relativistic particles, the sensitivity to m_X is more prominent at

	Frequentist	Bayesian
	Lyman- α ($z < 4.5$)+XQ-100	Lyman- α ($z < 4.5$)+XQ-100
T_0 ($z=3$) (10^3K)	13.9 ± 1.7	12.2 ± 2.0
γ	1.09 ± 0.13	1.01 ± 0.15
σ_8	0.796 ± 0.020	0.806 ± 0.021
n_s	0.954 ± 0.006	0.954 ± 0.006
Ω_m	0.265 ± 0.008	0.268 ± 0.009
m_X (keV , 95% CL)	> 5.3	> 5.9

Table 9. Preferred astrophysical and cosmological parameter values (68.3% confidence level) for the WDM model, for combined Lyman- α ($z < 4.5$) and XQ-100 data.

high redshift. Thus, the high-redshift data are the ones with the largest constraining power, despite having the largest statistical uncertainties. This feature is confirmed by the loosening of the bound as we restrict the data to lower redshifts. We obtain $m_X > 5.3$ keV for $z < 4.5$, and $m_X > 3.9$ keV for $z < 4.1$, both at 95% CL. This trend is also clearly visible in figure 8, where we show the χ^2 profiles for the three configurations. The profile widens (hence the constraint loosens) as we go from all redshifts (dark blue) to $z < 4.5$ (blue) then to $z < 4.1$ (light-blue).

The gain provided by the highest-redshift $z = 4.6$ bin, however, is two-fold. It is due in part because the $z = 4.6$ power spectrum probes structure growth in a more linear regime, but also because the minimum of the fit then occurs for $1 \text{ keV}/m_X < 0$. The Feldman-Cousins prescription [82] allows us to derive the limit in such a case, by computing the $\Delta\chi^2$ with respect to the χ^2 at the limit of the physical domain, i.e. where $1 \text{ keV}/m_X = 0$. This method, however, leads to an artificially strong limit, since the χ^2 profile in the physical ($m_X > 0$) region is a very steep function of $1 \text{ keV}/m_X$. To be conservative, we hence consider as our main result the bound obtained in the eBOSS DR14 ($z < 4.5$) + XQ-100 configuration: $m_X > 5.3$ keV (95% CL). We highlight the fact that removing the highest $z = 4.6$ redshift bin is sufficient to ensure that the best-fit minimum be in the physical region. Further data restriction does not alter its location. In table 9, we give the best-fit values of some of the main parameters with the two methodologies. We note an excellent agreement on all parameters.

These new bounds are significantly tighter than the 4.2 keV lower limit derived with BOSS DR9 ($z < 4.5$) + XQ-100 by [19] (red curve in figure 8). The improvement mostly comes from the improved statistical power of the eBOSS DR14 data compared to BOSS DR9, as is made clear by the comparison of the the limits obtained with the same $z < 4.5$ redshift range.

Because the IGM thermal history produces a cut-off in the flux power spectrum that is partially degenerate with the impact of a relativistic particle, we paid particular attention to the thermal modeling. The recovered $T_0(z)$, $\gamma(z)$ and mean flux are shown in appendix A. All three parameters are in perfect agreement with typical observed ranges. We also checked the impact of a different modeling by imposing a central thermal history in agreement with the observations of [40] and allowing variations in the amplitude and density dependence of the UV heating rates (AMPL and GRAD parameters of the hydrodynamical code GADGET).

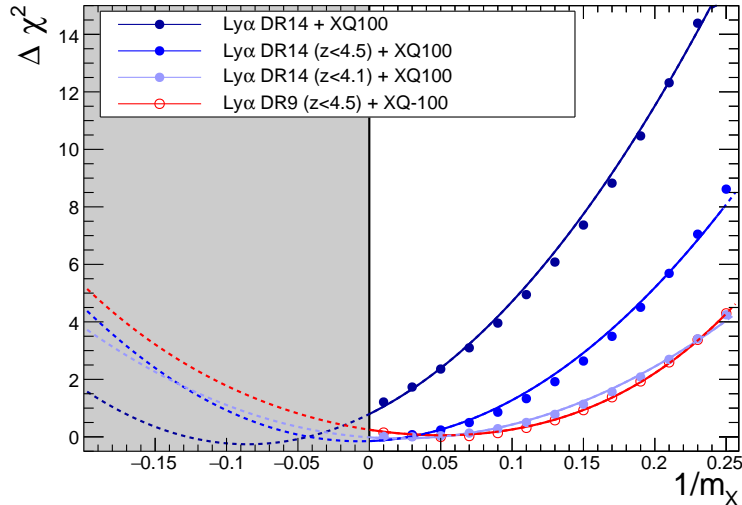


Figure 8. $\Delta\chi^2$ profile as a function of $1\text{keV}/m_X$ for the four configurations: Lyman- α + XQ-100 (dark blue), Lyman- α ($z < 4.5$) + XQ-100 (blue), Lyman- α ($z < 4.1$) + XQ-100 (light blue), DR9 Lyman- α ($z < 4.5$) + XQ-100 (red with open circles). Each point shows the $\Delta\chi^2$ obtained from a profiling method, i.e. after minimization over all other free parameters. The curves are the result of a parabolic fit to the points, extrapolated into the negative region.

This only had a mild impact on the constraints, which led to $m_X > 4.7\text{keV}$ for eBOSS ($z < 4.5$) + XQ-100. Finally, we give the correlation coefficients between the free parameters of the fit in appendix B. The $1/m_X$ parameter does not exhibit significant correlation with any of the parameters describing the thermal history.

As our most robust bound on WDM, we therefore take the eBOSS ($z < 4.5$) + XQ-100 configuration, marginalizing over the cosmological, astrophysical and nuisance parameters described in table 1. This leads to $m_X > 5.3\text{keV}$ (95% CL), or equivalently to a constraint on the mass of a non-resonantly produced sterile neutrino $m_s > 34\text{keV}$ (95% CL).

4 Conclusions

In this paper, we present an update of the constraints we derive on several cosmological parameters using Lyman- α data, either alone or in combination with CMB and BAO data. Compared to the previous study of PY15 [17], we update both large-scale and small-scale data sets: we use the most recent 1D Lyman- α flux power spectrum measured with the DR14 BOSS and eBOSS data of the SDSS, as well as the newest Planck 2018 data release.

We perform two statistical analyses in parallel: one based on a Bayesian and the other on a frequentist interpretation. The two approaches produce results that are in excellent agreement, demonstrating the robustness of the study. In order to be conservative, we choose to always report as our final result the largest (and hence weakest) bound, whether on the neutrino masses $\sum m_\nu$ or on the inverse of the mass of a thermal relic $1/m_X$.

We find a mild tension between the values of Ω_m preferred by the Lyman- α and the CMB data. Interestingly, the Lyman- α best-fit cosmological parameters are in very good agreement with current weak lensing constraints on (Ω_m, σ_8) . Lyman- α and weak lensing are two late-time probes of a similar range of scales, and they show a comparable level of tension with Planck Λ CDM model at the $2 - 3 \sigma$ level. Because Ω_m and n_s have a similar impact on the Lyman- α flux power spectrum, the small tension on Ω_m is likely to have the same origin as the mild tension on n_s previously observed by PY15 [17].

We performed comprehensive tests and did not identify a systematic effect in the data or in the analysis that would be the origin of this tension. However, we showed that it could be reduced by considering different scalar indices on CMB and Lyman- α scales, such as produced by a running of the scalar index. We find a mild preference for a non-zero running of n_s at the level of about 3σ : $dn_s/d \ln k \sim -0.010 \pm 0.004$. This detection is consistent with the previous study of PY15. It illustrates the small disagreement in the slopes of the power spectrum measured independently by BOSS/eBOSS and Planck.

The free-streaming of massive neutrinos causes a step-like suppression in the power spectrum that is ideally probed by comparing the large-scale CMB to the small scale Lyman- α power spectra. The constraint on $\sum m_\nu$ thus comes from the measurement of σ_8 in Lyman- α data, and from the correlation between σ_8 and $\sum m_\nu$ provided by CMB. The value of σ_8 is derived from the normalization of the 1D flux power spectrum, which is essentially unaffected by the inclusion or not of a variation in the slope of the power spectrum, as in the case of non-zero running.

Combining BOSS and eBOSS Lyman- α with Planck CMB data, we find an upper bound on $\sum m_\nu$ of 0.10 eV (95% CL) for a Λ CDM model, which only loosens to 0.11 eV when allowing for running. When further including CMB lensing and BAO, the limit tightens to $\sum m_\nu < 0.09$ eV, whether or not running is allowed. These limits improve slightly over those of PY15 and tend to favor the normal hierarchy neutrino mass scenario.

WDM affects clustering compared to the CDM scenario by suppressing all power below a scale determined by the particle mass. Thanks to the much improved statistics, the DR14 BOSS and eBOSS data allow us to improve the limit on WDM compared to previous publications. Using a combination of eBOSS ($z < 4.5$) + XQ-100 Lyman- α data, we constrain the mass m_X of a thermal relic to $m_X > 5.3$ keV (95% CL). It translates to a constraint on the mass m_s of a non-resonantly-produced sterile neutrino of $m_s > 34$ keV (95% CL).

The study presented in this work probably provides one of the most stringent bound on $\sum m_\nu$ that current high-statistics medium-resolution data can provide. WDM constraints, less sensitive to low-redshift data more prone to systematics, could still be further improved, for instance with additional high redshift data. We see two main paths for improvement in the near future. First, new-generation spectroscopic data from DESI, WEAVE, or 4MOST will soon be available. With a three to four-fold increase in quasar number density, it will be possible to further tighten the selection of the quasar spectra and reduce the contamination from systematic biases. With DESI, the factor of two gain in resolution and the reduced noise will improve the measurement on small scales relevant for $\sum m_\nu$. The extension of the DESI quasar selection to higher redshift is highly relevant to WDM. Secondly, improvements are also expected on the simulations side. The use of faster and less memory-intensive codes will allow one to run large-volume hydrodynamic cosmological resolution with the required

resolution without having to resort to splicing techniques. Emulator-based techniques can reduce the uncertainties in the model interpolation and bring them at the sub-percent level. Combined, these improvements should allow us to enter the era where $\sum m_\nu$ is no longer constrained but measured.

Acknowledgments

We would like to thank Marika Asgari, Hendrik Hildebrandt and Konrad Kuijken for sharing the results of their recent Weak Lensing data analysis with us. NS acknowledges support from the DFG grant LE 3742/4-1. JL is supported by the DFG grant LE 3742/3-1. MW, EA, NPD and CY acknowledge support from grant ANR-17-CE31- 0024-01 for the NILAC project. The Bayesian analysis was performed with computing resources granted by RWTH Aachen University under project jara0184. The hydrodynamical simulations were performed under PRACE allocations 2010PA2777, 2014102371 and 2012071264 and GENCI allocations t2013047004, t2016047706, A0030410313, A0050410586 on Curie thin and fat nodes at TGCC.

A Thermal history

We model the IGM thermal history through a set of parameters given in table 1. The recovered range of the IGM temperature $T(z)$, density dependence $\gamma(z)$ and mean flux $\bar{F}(z)$ are shown in figure 9 for the fits on the sum of the neutrino masses $\sum m_\nu$, and in figure 10 for the fit on the mass of a warm dark matter thermal relic. Current measurements of these parameters exhibit a wide spread. Values of T_0 vary among authors by over a factor 2 (typically between about 10 000K and 20 000K for redshifts between 2 and 3, decreasing with redshift to around 8 000K at $z = 4$), and γ can be found between 1.0 and 1.8 [43, 83, 84]. The central simulation of our simulation grid corresponds to the thermal model of [40]. For the purpose of this study, thermal parameters are taken as nuisance and we do not try to recover precise values. Instead, we allow for a lot of freedom in their range and modeling.

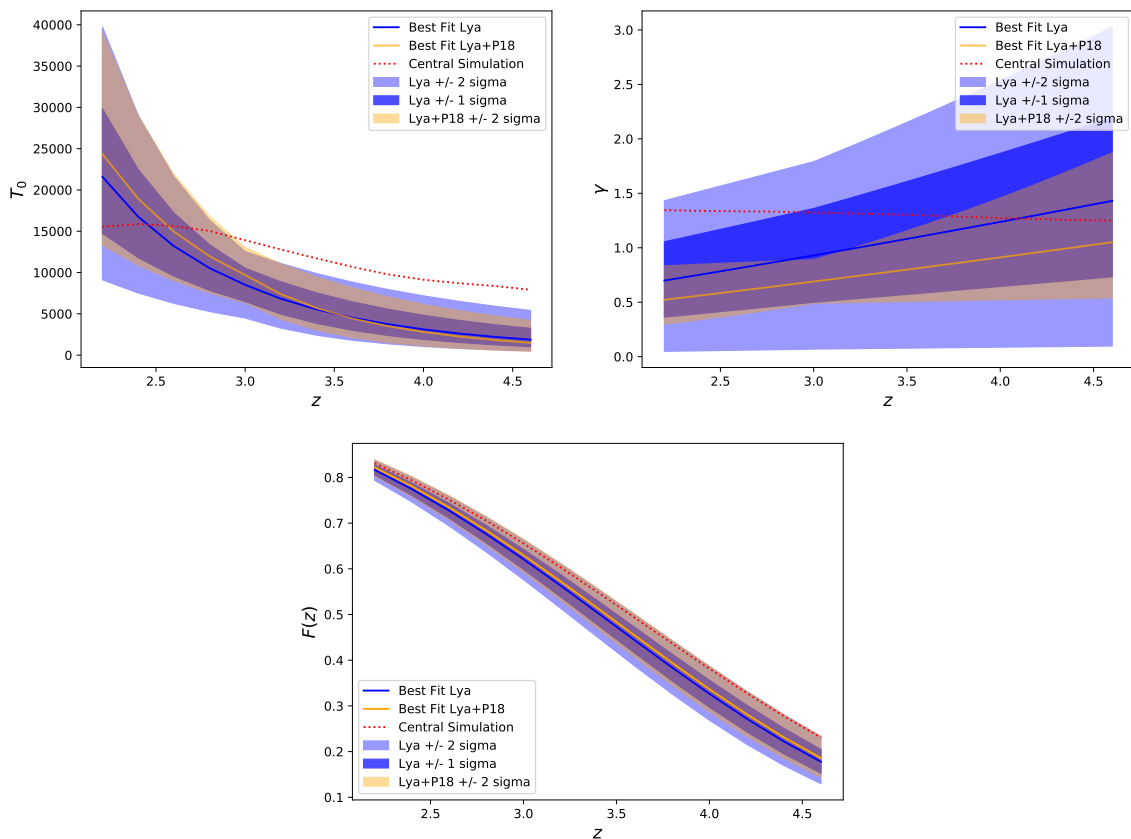


Figure 9. Thermal history for the $\sum m_\nu$ fit. Blue contours for Lyman- α data alone (1 and 2 σ contours), yellow for Lyman- α and Planck (2 σ contour only). The dashed red curve illustrates the thermal history of the central simulation of the grid. **Top left:** temperature $T_0(z)$. **Top right:** Density dependence $\gamma(z)$ parameter. **Bottom:** mean flux $\bar{F}(z)$.

In all fits, the recovered thermal history overlaps with the typical range allowed by observations. Warm dark matter fits are in perfect agreement with the central simulation on all three parameters. Neutrino mass fits tend to have a cold IGM at high redshift, although the 2 σ bound is within acceptable limits. Planck data do not constrain the IGM thermal

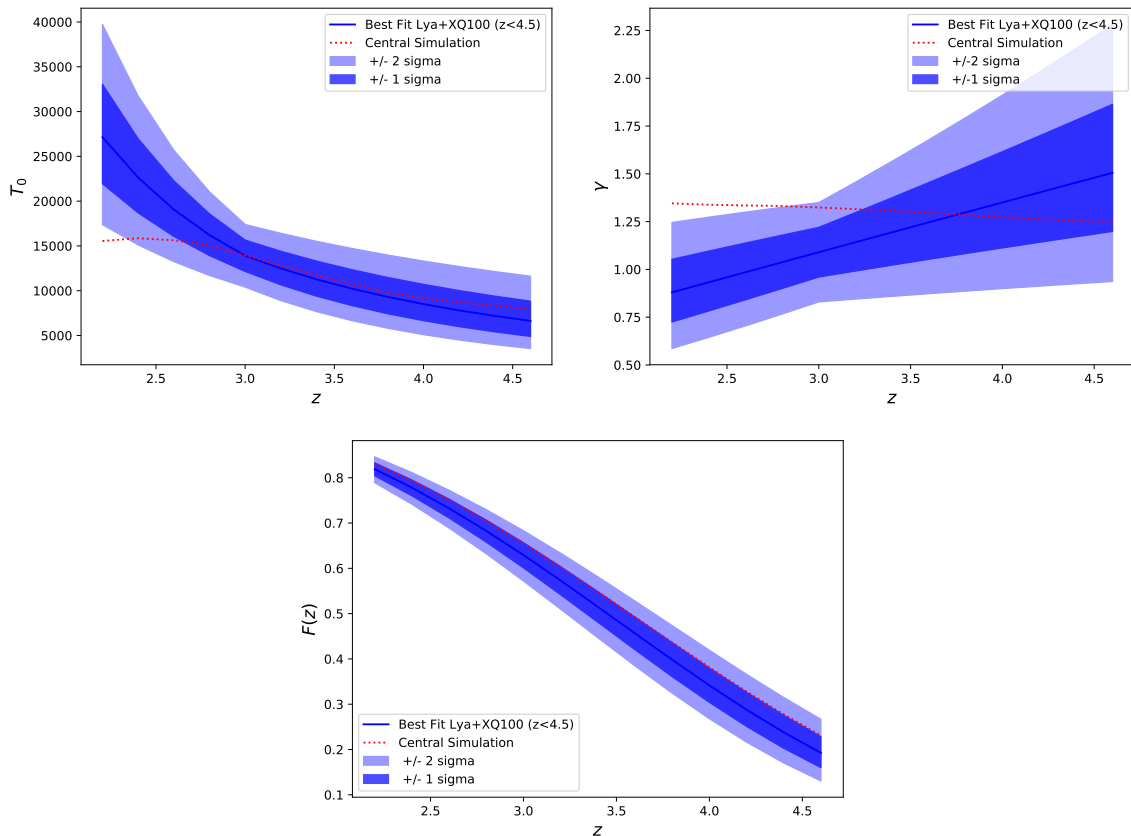


Figure 10. Thermal history for the m_X fit. Same color code as figure 9.

history. However, we note that adding them reduces the uncertainty on the thermal parameters through their correlation with cosmological parameters. The main impact is for γ , where its anti-correlation with Ω_M and n_s , combined with the light tension between Lyman- α and CMB data on these parameters, pushes it to low values in the Lyman- α +P18 neutrino mass fit. In contrast, Lyman- α data alone yield perfectly standard values of γ , T_0 and $\bar{F}(z)$.

To further check the robustness of our results, we tested a different, less flexible, thermal model. Instead of the one described by the parameters of table 1 that leave the slopes of the redshift-dependence free, we fixed the shape of the thermal history to that of [40] used in the central simulation, and we only allowed changes in amplitude and density dependence of the UV heating rates (AMPL and GRAD parameters of GADGET), effectively changing T_0 and γ at all redshifts. The limits obtained in this case are summarized in table 10. We note that the recovered thermal history is in excellent agreement with that of the central simulation in all cases. While considerably reduced, the trends noticed above when we included Planck data are still true (in particular a slightly lower value of γ). The bound on $\sum m_\nu$ is slightly tightened when imposing the more constrained thermal model. The looser fit of the paper therefore yields conservative bounds. The warm dark matter results are only mildly changed.

Configuration	Constraint (95% CL)	$T_0(z=3)$	$\gamma(z=3)$
Lyman- α	$\sum m_\nu < 0.39$ eV	7900K	1.1
Lyman- α + P18	$\sum m_\nu < 0.07$ eV	15700	1.0
Lyman- α ($z < 4.5$) + XQ100	$m_X > 4.7$ keV	13900	1.1

Table 10. Constraints on the sum of the neutrino masses and on the mass of WDM in the form of thermal relics assuming a thermal history following a similar shape as that of [40]. The last two columns give the equivalent T_0 and γ at redshift 3 for the best-fit model.

B Correlation coefficients

We provide the correlation coefficients between fit parameters in the case of the $\sum m_\nu$ fit to Lyman- α data alone in table 11, and in the case of the 1 keV/ m_X fit to Lyman- α ($z < 4.5$) + XQ100 data in table 12. For the sake of clarity, we restrict the table to matrix rows and columns that exhibit at least one coefficient with absolute value exceeding 25%, and we only show coefficients larger than 20% in absolute value.

	A^τ	η^τ	σ_8	n_s	T_0	γ	Ω_m	H_0	$\eta^T_{z < 3}$	$\eta^T_{z > 3}$	η^γ	A^{splice}	A^{AGN}
	0	1	2	3	4	5	6	7	8	9	10	11	12
0	1.												
1	-0.46	1.											
2	-	-	1.										
3	-0.48	-	-	1.									
4	-	-0.27	-0.35	0.38	1.								
5	0.25	0.39	-	-0.30	-0.60	1.							
6	-	-	0.39	-0.37	-0.23	-0.21	1.						
7	-	-	-	-0.30	-	-	-	1.					
8	-0.34	-	-0.43	0.43	0.62	-	-0.34	-	1.				
9	-	-	-	-	-	0.54	-	-	0.25	1.			
10	0.62	-0.58	-	-	0.24	-0.51	-	-	-0.41	-0.21	1.		
11	-	0.64	-0.25	-	-	0.27	-0.29	-	-	-	-	1.	
12	-	-	-	-0.39	-	-	-	-	-0.28	-0.22	-	-	1.

Table 11. Correlation coefficients for the $\sum m_\nu$ fit on Lyman- α . Only parameters with at least one correlation coefficient exceeding 25% in absolute value are shown, and we display all coefficients smaller than 0.20 in absolute value as “-”.

	A^τ	η^τ	n_s	T_0	γ	Ω_m	H_0	$\frac{1}{m_X}$	$\eta^T_{z < 3}$	$\eta^T_{z > 3}$	η^γ	A^{splice}	A^{AGN}	A^{SN}	z_{reio}
	0	1	2	3	4	5	6	7	8	9	10	11	12	13	14
0	1.														
1	-0.75	1.													
2	-0.45	0.42	1.												
3	-	-	-	1.											
4	-	0.24	-	-0.84	1.										
5	-	-	-0.41	-	-	1.									
6	-	-	-0.27	-	-	-	1.								
7	0.27	-0.32	-0.21	-	-	-	-	1.							
8	-	-0.35	-	-	-	-	-	-	1.						
9	-	-	-	-0.82	0.72	-	-	-	-	1.					
10	0.37	-	-	-	-0.40	-	-	-	-0.49	-0.28	1.				
11	-	0.46	0.33	-	-0.20	-	-	-	-0.51	-0.32	0.62	1.			
12	-	-	-0.37	-	-	-	-	-	-0.38	-	0.21	-	1.		
13	-	-	0.40	-	-	-	-	-	-	-0.31	-	-	-	-	-

Table 12. As table 11 for the WDM fit on Lyman- α ($z < 4.5$) + XQ100.

In the $\sum m_\nu$ fit, the cosmological parameters show correlation with some of the astrophysical or nuisance parameters, but never at a level exceeding 50%. The largest such correlations are between n_s and A^τ (-48%), between σ_8 and $\eta^T(z < 3)$ (-43%), and between

n_s and $\eta^T(z < 3)$ (43%). All other correlations with cosmological parameters are below 40%. In contrast, astrophysical and nuisance parameters show larger degeneracies, often in excess of 50% correlations. This is why, in particular, we do not have any claims on thermal history but instead consider parameters that describe it as nuisance, which we marginalize over (in the Bayesian approach) or leave free in the fit (in the frequentist approach).

In the WDM fit, m_X is only slightly correlated to the mean flux (27% with A^τ and -32% with η^τ) and to n_s (-21%). We find no significant correlation of m_X with any of the parameters describing the thermal history.

References

- [1] V. K. Narayanan, D. N. Spergel, R. Dave and C.-P. Ma, *Constraints on the mass of warm dark matter particles and the shape of the linear power spectrum from the Ly α forest*, *Astrophys. J.* **543** (2000) L103 [[astro-ph/0005095](#)].
- [2] M. Viel, J. Lesgourgues, M. G. Haehnelt, S. Matarrese and A. Riotto, *Constraining warm dark matter candidates including sterile neutrinos and light gravitinos with WMAP and the Lyman-alpha forest*, *Phys. Rev.* **D71** (2005) 063534 [[astro-ph/0501562](#)].
- [3] U. Seljak, A. Makarov, P. McDonald and H. Trac, *Can sterile neutrinos be the dark matter?*, *Phys. Rev. Lett.* **97** (2006) 191303 [[astro-ph/0602430](#)].
- [4] A. Boyarsky, J. Lesgourgues, O. Ruchayskiy and M. Viel, *Lyman-alpha constraints on warm and on warm-plus-cold dark matter models*, *JCAP* **0905** (2009) 012 [[0812.0010](#)].
- [5] C. Dvorkin, K. Blum and M. Kamionkowski, *Constraining Dark Matter-Baryon Scattering with Linear Cosmology*, *Phys. Rev.* **D89** (2014) 023519 [[1311.2937](#)].
- [6] W. L. Xu, C. Dvorkin and A. Chael, *Probing sub-GeV Dark Matter-Baryon Scattering with Cosmological Observables*, *Phys. Rev.* **D97** (2018) 103530 [[1802.06788](#)].
- [7] M. Garny, T. Konstandin, L. Sagunski and S. Tulin, *Lyman- α forest constraints on interacting dark sectors*, *JCAP* **1809** (2018) 011 [[1805.12203](#)].
- [8] SDSS collaboration, *Cosmological parameter analysis including SDSS Ly-alpha forest and galaxy bias: Constraints on the primordial spectrum of fluctuations, neutrino mass, and dark energy*, *Phys. Rev.* **D71** (2005) 103515 [[astro-ph/0407372](#)].
- [9] U. Seljak, A. Slosar and P. McDonald, *Cosmological parameters from combining the Lyman-alpha forest with CMB, galaxy clustering and SN constraints*, *JCAP* **0610** (2006) 014 [[astro-ph/0604335](#)].
- [10] J. Baur, N. Palanque-Delabrouille, C. Yèche, C. Magneville and M. Viel, *Lyman-alpha forests cool warm dark matter*, *JCAP* **8** (2016) 012 [[1512.01981](#)].
- [11] J. Baur, N. Palanque-Delabrouille, C. Yèche, A. Boyarsky, O. Ruchayskiy, É. Armengaud et al., *Constraints from Ly- α forests on non-thermal dark matter including resonantly-produced sterile neutrinos*, *JCAP* **12** (2017) 013 [[1706.03118](#)].
- [12] V. Iršič, M. Viel, M. G. Haehnelt, J. S. Bolton, S. Cristiani, G. D. Becker et al., *New constraints on the free-streaming of warm dark matter from intermediate and small scale Lyman- α forest data*, *Phys. Rev. D* **96** (2017) 023522 [[1702.01764](#)].
- [13] V. Iršič, M. Viel, M. G. Haehnelt, J. S. Bolton and G. D. Becker, *First Constraints on Fuzzy Dark Matter from Lyman- α Forest Data and Hydrodynamical Simulations*, *Physical Review Letters* **119** (2017) 031302 [[1703.04683](#)].

- [14] E. Armengaud, N. Palanque-Delabrouille, C. Yèche, D. J. E. Marsh and J. Baur, *Constraining the mass of light bosonic dark matter using SDSS Lyman- α forest*, *MNRAS* **471** (2017) 4606 [[1703.09126](#)].
- [15] U. Seljak, A. Slosar and P. McDonald, *Cosmological parameters from combining the Lyman- α forest with CMB, galaxy clustering and SN constraints*, *Journal of Cosmology and Astroparticle Physics* **10** (2006) 14 [[astro-ph/0604335](#)].
- [16] M. Viel, M. G. Haehnelt and V. Springel, *The effect of neutrinos on the matter distribution as probed by the intergalactic medium*, *Journal of Cosmology and Astroparticle Physics* **2010** (2010) 015 [[1003.2422](#)].
- [17] N. Palanque-Delabrouille et al., *Neutrino masses and cosmology with Lyman-alpha forest power spectrum*, *JCAP* **1511** (2015) 011 [[1506.05976](#)].
- [18] N. Palanque-Delabrouille et al., *Constraint on neutrino masses from SDSS-III/BOSS Ly α forest and other cosmological probes*, *JCAP* **1502** (2015) 045 [[1410.7244](#)].
- [19] C. Yèche, N. Palanque-Delabrouille, J. Baur and H. du Mas des Bourboux, *Constraints on neutrino masses from Lyman-alpha forest power spectrum with BOSS and XQ-100*, *JCAP* **6** (2017) 047 [[1702.03314](#)].
- [20] S. Chabanier, N. Palanque-Delabrouille, C. Yèche, J.-M. Le Goff, E. Armengaud, J. Bautista et al., *The one-dimensional power spectrum from the SDSS DR14 Ly α forests*, *arXiv e-prints* (2018) arXiv:1812.03554 [[1812.03554](#)].
- [21] K. S. Dawson, D. J. Schlegel, C. P. Ahn, S. F. Anderson, E. Aubourg, S. Bailey et al., *The Baryon Oscillation Spectroscopic Survey of SDSS-III*, *The Astronomical Journal* **145** (2013) 10 [[1208.0022](#)].
- [22] K. S. Dawson, J.-P. Kneib, W. J. Percival, S. Alam, F. D. Albareti, S. F. Anderson et al., *The SDSS-IV Extended Baryon Oscillation Spectroscopic Survey: Overview and Early Data*, *AJ* **151** (2016) 44 [[1508.04473](#)].
- [23] A. Borde, N. Palanque-Delabrouille, G. Rossi, M. Viel, J. S. Bolton, C. Yèche et al., *New approach for precise computation of Lyman- α forest power spectrum with hydrodynamical simulations*, *JCAP* **7** (2014) 005 [[1401.6472](#)].
- [24] I. Pâris, P. Petitjean, É. Aubourg, A. D. Myers, A. Streblyanska, B. W. Lyke et al., *The Sloan Digital Sky Survey Quasar Catalog: Fourteenth data release*, *A&A* **613** (2018) A51 [[1712.05029](#)].
- [25] N. P. Ross, A. D. Myers, E. S. Sheldon, C. Yèche, M. A. Strauss, J. Bovy et al., *The SDSS-III Baryon Oscillation Spectroscopic Survey: Quasar Target Selection for Data Release Nine*, *The Astrophysical Journal Suppl.* **199** (2012) 3 [[1105.0606](#)].
- [26] A. D. Myers, N. Palanque-Delabrouille, A. Prakash, I. Pâris, C. Yèche, K. S. Dawson et al., *The SDSS-IV Extended Baryon Oscillation Spectroscopic Survey: Quasar Target Selection*, *ApJS* **221** (2015) 27 [[1508.04472](#)].
- [27] N. Palanque-Delabrouille, C. Magneville, C. Yèche, I. Pâris, P. Petitjean, E. Burtin et al., *The extended Baryon Oscillation Spectroscopic Survey: Variability selection and quasar luminosity function*, *A&A* **587** (2016) A41 [[1509.05607](#)].
- [28] N. Palanque-Delabrouille, C. Yèche, J. Baur, C. Magneville, G. Rossi, J. Lesgourgues et al., *Neutrino masses and cosmology with Lyman-alpha forest power spectrum*, *JCAP* **11** (2015) 011 [[1506.05976](#)].
- [29] PLANCK collaboration, *Planck 2018 results. V. CMB power spectra and likelihoods*, [1907.12875](#).

- [30] F. Beutler, C. Blake, M. Colless, D. H. Jones, L. Staveley-Smith, L. Campbell et al., *The 6dF Galaxy Survey: baryon acoustic oscillations and the local Hubble constant*, *MNRAS* **416** (2011) 3017 [1106.3366].
- [31] A. J. Ross et al., *The Clustering of Galaxies in the SDSS-III DR10 Baryon Oscillation Spectroscopic Survey: No Detectable Colour Dependence of Distance Scale or Growth Rate Measurements*, *Mon. Not. Roy. Astron. Soc.* **437** (2014) 1109 [1310.1106].
- [32] S. Alam, M. Ata, S. Bailey, F. Beutler, D. Bizyaev, J. A. Blazek et al., *The clustering of galaxies in the completed SDSS-III Baryon Oscillation Spectroscopic Survey: cosmological analysis of the DR12 galaxy sample*, *MNRAS* **470** (2017) 2617 [1607.03155].
- [33] G. Rossi, N. Palanque-Delabrouille, A. Borde, M. Viel, C. Yèche, J. S. Bolton et al., *Suite of hydrodynamical simulations for the Lyman- α forest with massive neutrinos*, *A & A* **567** (2014) A79 [1401.6464].
- [34] V. Springel, N. Yoshida and S. D. White, *GADGET: a code for collisionless and gasdynamical cosmological simulations*, *New Astronomy* **6** (2001) 79 [0003162].
- [35] V. Springel, *The cosmological simulation code GADGET-2*, *Monthly Notices of the Royal Astronomical Society* **364** (2005) 1105 [0505010].
- [36] A. Lewis, A. Challinor and A. Lasenby, *Efficient Computation of Cosmic Microwave Background Anisotropies in Closed Friedmann-Robertson-Walker Models*, *The Astrophysical Journal* **538** (2000) 473 [9911177].
- [37] P. McDonald, *Toward a Measurement of the Cosmological Geometry at $z \sim 2$: Predicting Ly-alpha Forest Correlation in Three Dimensions and the Potential of Future Data Sets*, *The Astrophysical Journal* **585** (2003) 34 [0108064].
- [38] PLANCK collaboration, *Planck 2013 results. XVI. Cosmological parameters*, *Astron. Astrophys.* **571** (2014) A16 [1303.5076].
- [39] A. A. Meiksin, *The physics of the intergalactic medium*, *Reviews of Modern Physics* **81** (2009) 1405 [0711.3358].
- [40] G. D. Becker, J. S. Bolton, M. G. Haehnelt and W. L. W. Sargent, *Detection of extended HeII reionization in the temperature evolution of the intergalactic medium*, *Monthly Notices of the Royal Astronomical Society* **410** (2011) 1096 [1008.2622].
- [41] L. Hui and N. Y. Gnedin, *Equation of state of the photoionized intergalactic medium*, *Mon. Not. Roy. Astron. Soc.* **292** (1997) 27 [astro-ph/9612232].
- [42] T. Theuns, *Numerical simulations of quasar absorbers*, in *IAU Colloq. 199: Probing Galaxies through Quasar Absorption Lines*, P. Williams, C.-G. Shu and B. Menard, eds., pp. 185–204, Mar., 2005, astro-ph/0507570, DOI.
- [43] M. Walther, J. Oñorbe, J. F. Hennawi and Z. Lukić, *New Constraints on IGM Thermal Evolution from the Ly α Forest Power Spectrum*, *ApJ* **872** (2019) 13 [1808.04367].
- [44] E. Puchwein, J. S. Bolton, M. G. Haehnelt, P. Madau, G. D. Becker and F. Haardt, *The photoheating of the intergalactic medium in synthesis models of the UV background*, *Mon. Not. Roy. Astron. Soc.* **450** (2015) 4081 [1410.1531].
- [45] S. Chabanier et al., *The impact of AGN feedback on the 1D power spectra from the Ly-alpha forests using the Horizon-AGN simulation*, (in prep) (2019) .
- [46] M. Viel, J. Schaye and C. M. Booth, *The impact of feedback from galaxy formation on the Lyman α transmitted flux*, *Monthly Notices of the Royal Astronomical Society* **429** (2013) 1734 [1207.6567].
- [47] J. Neyman, *Outline of a Theory of Statistical Estimation Based on the Classical Theory of Probability*, *Trans. Royal Soc. London, Series A* **236** (1937) 333.

- [48] T. Brinckmann and J. Lesgourgues, *MontePython 3: boosted MCMC sampler and other features*, [1804.07261](#).
- [49] PARTICLE DATA GROUP collaboration, *Review of Particle Physics*, *Phys. Rev.* **D98** (2018) 030001.
- [50] J. F. Beacom, N. F. Bell and S. Dodelson, *Neutrinoless universe*, *Phys. Rev. Lett.* **93** (2004) 121302 [[astro-ph/0404585](#)].
- [51] Z. Chacko, A. Dev, P. Du, V. Poulin and Y. Tsai, *Cosmological Limits on the Neutrino Mass and Lifetime*, [1909.05275](#).
- [52] S. Roy Choudhury and S. Hannestad, *Updated results on neutrino mass and mass hierarchy from cosmology with Planck 2018 likelihoods*, [1907.12598](#).
- [53] Planck Collaboration, P. A. R. Ade, N. Aghanim, M. Arnaud, M. Ashdown, J. Aumont et al., *Planck 2015 results. XIII. Cosmological parameters*, *ArXiv:1502.01589* (2015) [[1502.01589](#)].
- [54] Planck Collaboration, N. Aghanim, Y. Akrami, M. Ashdown, J. Aumont, C. Baccigalupi et al., *Planck 2018 results. VI. Cosmological parameters*, *ArXiv e-prints* (2018) [[1807.06209](#)].
- [55] A. G. Riess, S. Casertano, W. Yuan, L. M. Macri and D. Scolnic, *Large Magellanic Cloud Cepheid Standards Provide a 1% Foundation for the Determination of the Hubble Constant and Stronger Evidence for Physics beyond Λ CDM*, *Astrophys. J.* **876** (2019) 85 [[1903.07603](#)].
- [56] M. Asgari et al., *KiDS+VIKING-450 and DES-Y1 combined: Mitigating baryon feedback uncertainty with COSEBIs*, [1910.05336](#).
- [57] DES collaboration, *Dark Energy Survey Year 1 results: Cosmological constraints from cosmic shear*, *Phys. Rev.* **D98** (2018) 043528 [[1708.01538](#)].
- [58] S. Joudaki et al., *KiDS+VIKING-450 and DES-Y1 combined: Cosmology with cosmic shear*, [1906.09262](#).
- [59] C. Laigle et al., *The COSMOS2015 Catalog: Exploring the $1 < z < 6$ Universe with half a million galaxies*, *Astrophys. J. Suppl.* **224** (2016) 24 [[1604.02350](#)].
- [60] DES collaboration, *Dark Energy Survey Year 1 Results: Photometric Data Set for Cosmology*, *Astrophys. J. Suppl.* **235** (2018) 33 [[1708.01531](#)].
- [61] DES collaboration, *Dark Energy Survey Year 1 Results: Weak Lensing Shape Catalogues*, *Mon. Not. Roy. Astron. Soc.* **481** (2018) 1149 [[1708.01533](#)].
- [62] A. H. Wright et al., *KiDS+VIKING-450: A new combined optical & near-IR dataset for cosmology and astrophysics*, [1812.06077](#).
- [63] K. K. Rogers, S. Bird, H. V. Peiris, A. Pontzen, A. Font-Ribera and B. Leistedt, *Simulating the effect of high column density absorbers on the one-dimensional Lyman α forest flux power spectrum*, *MNRAS* **474** (2018) 3032 [[1706.08532](#)].
- [64] P. McDonald, U. Seljak, R. Cen, D. Shih, D. H. Weinberg, S. Burles et al., *The Linear Theory Power Spectrum from the Ly-alpha Forest in the Sloan Digital Sky Survey*, *The Astrophysical Journal* **635** (2005) 761 [[0407377](#)].
- [65] A. Kosowsky and M. S. Turner, *CBR anisotropy and the running of the scalar spectral index*, *Phys. Rev. D* **52** (1995) 1739 [[astro-ph/9504071](#)].
- [66] M. Joy, V. Sahni and A. A. Starobinsky, *A New Universal Local Feature in the Inflationary Perturbation Spectrum*, *Phys. Rev.* **D77** (2008) 023514 [[0711.1585](#)].
- [67] M. A. Buen-Abad, G. Marques-Tavares and M. Schmaltz, *Non-Abelian dark matter and dark radiation*, *Phys. Rev.* **D92** (2015) 023531 [[1505.03542](#)].
- [68] H. Motohashi, A. A. Starobinsky and J. Yokoyama, *$f(R)$ Gravity and its Cosmological Implications*, *Int. J. Mod. Phys.* **D20** (2011) 1347 [[1101.0716](#)].

- [69] T. Kobayashi and F. Takahashi, *Running spectral index from inflation with modulations*, *JCAP* **01** (2011) 026 [[1011.3988](#)].
- [70] L. McAllister, E. Silverstein and A. Westphal, *Gravity waves and linear inflation from axion monodromy*, *Phys.Rev.D* **82** (2010) 046003 [[0808.0706](#)].
- [71] G. Hinshaw, D. Larson, E. Komatsu, D. N. Spergel, C. L. Bennett, J. Dunkley et al., *Nine-year Wilkinson Microwave Anisotropy Probe (WMAP) Observations: Cosmological Parameter Results*, *ApJS* **208** (2013) 19 [[1212.5226](#)].
- [72] J. L. Sievers, R. A. Hlozek, M. R. Nolta, V. Acquaviva, G. E. Addison, P. A. R. Ade et al., *The Atacama Cosmology Telescope: cosmological parameters from three seasons of data*, *JCAP* **10** (2013) 60 [[1301.0824](#)].
- [73] Z. Hou, C. L. Reichardt, K. T. Story, B. Follin, R. Keisler, K. A. Aird et al., *Constraints on Cosmology from the Cosmic Microwave Background Power Spectrum of the 2500 deg² SPT-SZ Survey*, *ApJ* **782** (2014) 74 [[1212.6267](#)].
- [74] J. Lesgourgues and S. Pastor, *Massive neutrinos and cosmology*, *Phys.Rept.* **429** (2006) 307 [[astro-ph/0603494](#)].
- [75] J. Lesgourgues, G. Mangano, G. Miele and S. Pastor, *Neutrino Cosmology*. Cambridge University Press, 2013.
- [76] PARTICLE DATA GROUP collaboration, *Review of particle physics*, *Phys. Rev. D* **98** (2018) 030001.
- [77] P. F. de Salas, D. V. Forero, C. A. Ternes, M. Tórtola and J. W. F. Valle, *Status of neutrino oscillations 2018: 3 σ hint for normal mass ordering and improved CP sensitivity*, *Physics Letters B* **782** (2018) 633.
- [78] S. Dodelson and L. M. Widrow, *Sterile neutrinos as dark matter*, *Phys. Rev. Lett.* **72** (1994) 17 [[hep-ph/9303287](#)].
- [79] A. Boyarsky, J. Lesgourgues, O. Ruchayskiy and M. Viel, *Lyman- α constraints on warm and on warm-plus-cold dark matter models*, *JCAP* **5** (2009) 12 [[0812.0010](#)].
- [80] A. Garzilli, A. Boyarsky and O. Ruchayskiy, *Cutoff in the Lyman $\{\alpha\}$ forest power spectrum: warm IGM or warm dark matter?*, *ArXiv e-prints* (2015) [[1510.07006](#)].
- [81] A. Garzilli, A. Magalich, T. Theuns, C. S. Frenk, C. Weniger, O. Ruchayskiy et al., *The Lyman- α forest as a diagnostic of the nature of the dark matter*, *MNRAS* **489** (2019) 3456 [[1809.06585](#)].
- [82] G. J. Feldman and R. D. Cousins, *Unified approach to the classical statistical analysis of small signals*, *Physical Review D* **57** (1998) 3873 [[physics/9711021](#)].
- [83] H. Hiss, M. Walther, J. F. Hennawi, J. Oñorbe, J. M. O’Meara, A. Rorai et al., *A New Measurement of the Temperature-density Relation of the IGM from Voigt Profile Fitting*, *ApJ* **865** (2018) 42 [[1710.00700](#)].
- [84] A. Lidz and M. Malloy, *On Modeling and Measuring the Temperature of the $z \sim 5$ Intergalactic Medium*, *ApJ* **788** (2014) 175 [[1403.6350](#)].